INVITED PAPER

Graph-Theoretic Analysis of Power Systems

This article provides a comprehensive overview of the applications of graph theory in power system modeling, dynamics, coherency, and control.

By Takayuki Ishizaki, *Member IEEE*, Aranya Chakrabortty, *Senior Member IEEE*, and Jun-Ichi Imura, *Senior Member IEEE*

ABSTRACT | In this paper, we present an overview of the applications of graph theory in power system modeling, dynamics, coherency, and control. First, we study synchronization of generator dynamics using both nonlinear and small-signal representations of classical structure-preserving models of power systems in light of their network structure and the weights associated with the nodes and edges of the network graph. We overview important necessary and sufficient conditions for both phase and frequency synchronization. We highlight the role of graph structure in coherency properties, and introduce the idea of generator and bus aggregation whereby dynamic equivalent models of large power grids can be developed while retaining the concept of a "bus" in the network graph of the equivalent model. We also discuss several new results on graph sparsification for designing distributed controllers for power flow oscillation damping.

KEYWORDS | Graph theory; modeling; power systems; stability; structured control; topology

I. INTRODUCTION

Over the past decade power systems in different parts of the world have encountered a series of cascading failures and blackouts, starting from the major blackout in the Northeastern United States in 2003 to Hurricane Katrina in New Orleans in 2005, the European blackouts of 2006, the southwest blackout in San Diego and Tijuana in 2011, the recent natural disasters in Texas and Puerto Rico, and many other similar calamities and power outages in other corners of the globe. These blackouts have forced power system researchers to look beyond the traditional approach of analyzing power system functionalities in steady-state, and instead pay serious attention to their dynamic characteristics, and that too in a global and structural sense [1]. At the fundamental level, a power system is an interconnected network of electrical generators, loads, and their associated control elements. Each of these components may be thought of as nodes of a graph, while the transmission lines connecting them physically can be regarded as the edges of the graph. The nodes are modeled by physical laws that typically lead to a set of differential equations. These differential equations are coupled to each other by so-called power balance across the tie lines or the edges. One primary issue that has been of interest to power engineers over many years is how the graph-theoretic properties of these types of electrical networks impact the stability, dynamic performance, controllability, observability, identifiability, and other system-theoretic properties of the grid model [2]. These issues have been partly addressed in a handful of papers in the literature. For example, notions of structure-preserving models were laid out in the early 1980s in [3], followed by graph-theoretic analysis of transient stability using Lyapunov stability theory [4], [5]. But a systematic understanding of how graph theory can serve as a tool for deeper understanding of power system dynamics, stability, and control is still a large open question.

These topics have emerged with renewed interest in recent years, mainly owing to the expansion of transmission network in the United States [6], Asia [7], and Europe [8], and also due to intrusion of renewable energy sources [9]. In [10], for example, it was shown that if injected beyond a certain upper limit, and if not controlled accurately, wind power can easily cause transient instability in a conventional power grid. Both the amount of wind power and the precise location of injection matter. From a graph-theoretic perspective this means that synchronization of a homogeneous network of nonlinear oscillators can easily

Manuscript received October 30, 2017; revised February 8, 2018; accepted February 12, 2018. Date of current version April 24, 2018. The work of A. Chakrabortty was supported in part by the U.S. National Science Foundation (NSF) under Grant ECCS 1711004. The work of T. Ishizaki and J.-I. Imura was supported by the Japan Science and Technology Agency (JST) Core Research for Evolutional Science and Technology (CREST) program under Grant JPMJCR15K1. *(Corresponding author: Aranya Chakrabortty.)*

T. Ishizaki and **J.-I. Imura** are with the School of Engineering, Tokyo Institute of Technology, Tokyo 152-8552, Japan (e-mail: ishizaki@sc.e.titech.ac.jp; imura@sc.e.titech.ac.jp).

A. Chakrabortty is with the Computer Engineering, North Carolina State University, Raleigh, NC 27695 USA (e-mail: achakra2@ncsu.edu).

Digital Object Identifier: 10.1109/JPROC.2018.2812298

be perturbed and destabilized if any heterogeneous dynamics is injected into this network at the wrong node, and in the wrong amount. Similar structural implications have also been made for system identification of reduced-order models [11], optimal power flow [12], [13], voltage stability [14], and bifurcations [15]. Power engineers are currently seeking various ways to gain insight about the structural properties of their systems, which, in turn, can help in better synchronization and stability [16], observability [17], sensor placement [18], and control [19], [20].

Motivated by this gap, in this tutorial, we present several existing and new results on the applications of graph theory in power systems. Our results cover modeling, stability analysis, and control, highlighting the implications of the structure and the parameters associated with the underlying network graph. To keep the article compact, we mostly focus on angle stability and frequency stability, where graph theory plays a significant role. Discussion on voltage stability is skipped for brevity. The interested reader is referred to [21] and [22] for a review of voltage stability, and its connection with network cutsets. We start with a brief primer on hypothetical mass-spring-damper models, which represent swing dynamics or Newton's second law of motion in the models of synchronous generators. We show how the state-space representations of these models are explicit functions of the network topology. Thereafter, we extend the discussion to more realistic grid models consisting of both generator and nongenerator buses, and derive the notion of Kron reduction by which the differential-algebraic model of the grid can be represented as an ordinary differential equation model with certain compromises in the underlying network structure. We discuss the impacts of this reduction on the existence of power system equilibrium and its stability. We also derive small-signal linearization of this nonlinear model, and show that the synchronization properties of the generator states are strongly dependent on the symmetry properties of the underlying graph. We use this observation to define the concept of generator and bus aggregation, the latter being a new result that has not been studied so far in the power system literature. We illustrate the idea of aggregation for various symmetries and the asymmetries of the network graph using simulations. Finally, we show how structured distributed controllers can be designed for power oscillation damping in grid models using ideas from graph sparsification.

Notation: We denote the set of real values by $\mathbb{R}$, the set of nonnegative real values by $\mathbb{R}_{\geq 0}$, the unit circle by $\mathbb{S}$, the n-dimensional identity matrix by I_n, the ith column of I_n by e_i, the diagonal or block diagonal matrix whose ith diagonal entry is d_i by $\mathrm{diag}\,(d_i)_{i\in\{1,\ldots,n\}}$, the n-dimensional all-ones vector by $\mathbb{1}_n$, the image of a matrix A by $\mathrm{im}\,A$, the Hadamard product (i.e., the element-wise product) of vectors v and u by $v \circ u$, the Kronecker product of matrices A and B by $A \otimes B$, the cardinality of a set $\mathcal{S}$ by $|\mathcal{S}|$. For a matrix $A \in \mathbb{R}^{n\times m}$

$$\mathrm{diag}(A) := \mathrm{diag}\,\left(e_i^\mathsf{T} A\right)_{i\in\{1,\ldots,n\}} \in \mathbb{R}^{n\times nm}$$

where $e_i^\mathsf{T} A$ corresponds to the ith row of A. For a vector $\theta \in \mathbb{S}^n$, the trigonometric functions $\mathbf{sin}\theta$ and $\mathbf{cos}\theta$ are defined in the element-wise sense. Every complex-valued matrix or vector is denoted by a bold face symbol like $\boldsymbol{V}$. The imaginary unit $\sqrt{-1}$ is denoted by $\mathbf{i}$. A symmetric matrix $A = A^\mathsf{T}$ is said to be positive definite (respectively, positive semidefinite) if all eigenvalues of A are positive (nonnegative). A symmetric matrix $A = A^\mathsf{T} \in \mathbb{R}^{n\times n}$ is said to be a weighted graph Laplacian if its off-diagonal elements are all nonpositive and $A\mathbb{1}_n = 0$.

II. MASS-SPRINGER-DAMPER MODELS OF POWER SYSTEMS

The first step of understanding power system dynamics is to understand the dynamics of the electromechanical behavior of synchronous machines, which is really nothing but a study of how a group of nonlinear pendula would oscillate with respect to each other when they are connected over a given connection topology; in other words, how a set of mass-spring-damper systems, each of which has its own individual local frequencies of oscillations, would start oscillating against each other, and define a global oscillatory behavior when connected together in some combinations. The actual model of a synchronous machine is, of course, much more complex [23], but the mass-spring-damper model is the simplest example for describing its electromechanical dynamics. The mass here is analogous to a synchronous generator with a nonzero inertia. The spring is analogous to a transmission line that connects one generator to another. The damper is analogous to the internal damping mechanisms of a synchronous generator that ensures asymptotic stability of its state responses after a disturbance. The only difference, of course, is that unlike a mass-spring-damper system where the masses exhibit mechanical motion, the motion of a synchronous generator pertains to electrical motion, not mechanical. A comparison between mass-springer systems and power systems is shown in Fig. 1 using a 2-mass and a 2-generator example.

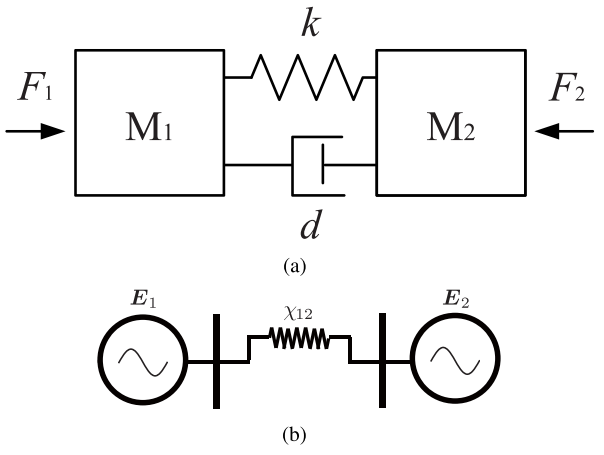

Fig. 1. ***Mass-spring-damper models of synchronous machines. (a) Mass spring damper. (b) Two interconnected synchronous machines.***

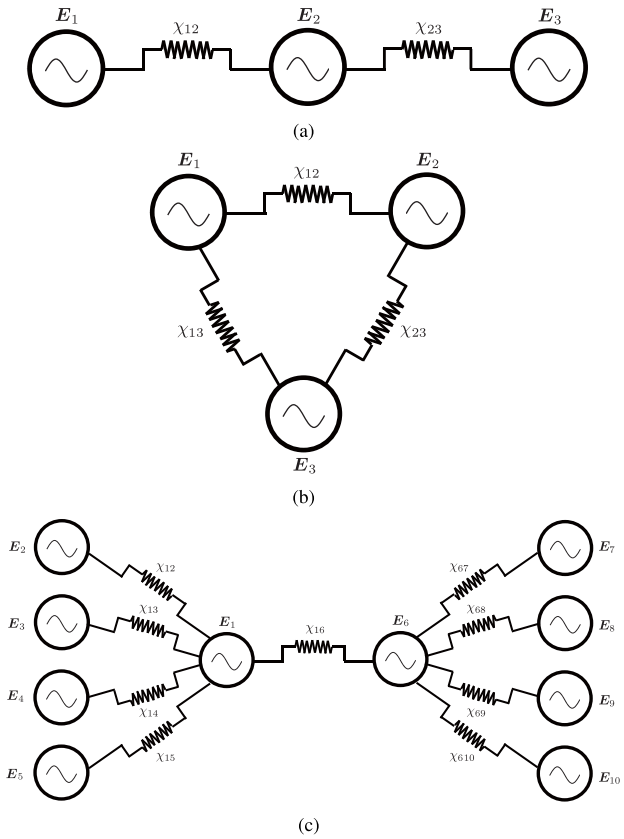

Fig. 2. ***Examples of mass-spring-damper representations of power systems. (a) Three generators in radial connection. (b) Three generators in loop connection. (c) System with ten generators.***

The starting point in deriving these mass-spring-damper models is the so-called swing equation of a synchronous generator. Consider the total number of generators to be n that are connected to each other in some given topology. Examples of systems with $n = 3$, connected in both radial and loop topology, and $n = 10$ following this kind of an idealistic model are shown in Fig. 2. The rotor of the generator is rotated by a prime mover, which in this case is a steam turbine. For $i = 1, \ldots, n$, Newton's second law of motion (mass times acceleration equals net force) in angular coordinates results in the swing equations [23]

$$\begin{aligned} \dot{\delta}_i(t) &= \tilde{\omega}_i(t) - \omega_s \\ M_i \dot{\tilde{\omega}}_i(t) &= P_{mi}(t) - P_{gi}(t) \end{aligned} \tag{1}$$

where the state variable δ_i is the phase angle of the rotor of the ith generator; the state variable $\tilde{\omega}_i$ is the velocity of the rotor of the ith generator with respect to a fixed reference frame (following the theory of electric machines, the reference for measuring δ_i, for example, can be taken to be the a-phase axis in the three-phase representation of the classical model of the synchronous generator circuit); ω_s is the synchronous frequency whose value is $120\pi = 377$ rad/s for a 60-Hz system; P_{gi} is the active power produced by the ith generator; M_i is the ith inertia constant; and P_{mi} is the mechanical power input from the ith turbine.

All quantities are normalized following the per unit representation of power system models [23]. If the generator has a nonzero damping factor $d_i > 0$, then the model can be written as

$$\begin{aligned} \dot{\delta}_i(t) &= \tilde{\omega}_i(t) - \omega_s \\ M_i \dot{\tilde{\omega}}_i(t) &= P_{mi}(t) - d_i(\tilde{\omega}_i(t) - \omega_s) - P_{gi}(t) \end{aligned} \tag{2}$$

which is referred to as the "swing equations" of the ith generator. The turbine power P_{mi} can either be set to a constant value, or used as a control input to regulate the generator dynamics, for example, in automatic generation control (AGC) [23]. Denoting $\omega_i(t) = \tilde{\omega}_i(t) - \omega_s$, a more compact form of the swing equation can be written as

$$\begin{aligned} \dot{\delta}_i(t) &= \omega_i(t) \\ M_i \dot{\omega}_i(t) &= P_{mi}(t) - d_i \omega_i(t) - P_{gi}(t). \end{aligned} \tag{3}$$

To generate a state-space model for the system out of the individual generator model (3), we next apply Ohm's law and Kirchoff's law to relate the active power P_{gi} to the rest of the grid. For simplicity, we drop the time argument t. By definition, P_{gi} can be written as

$$P_{gi} = \mathrm{Re}\left(\boldsymbol{E}_i \boldsymbol{I}_i^*\right) \tag{4}$$

where $\boldsymbol{I}_i \in \mathbb{C}$ is the total current in the complex phasor form produced by the ith generator, $*$ indicates the complex conjugate, and $\boldsymbol{E}_i \in \mathbb{C}$ is the voltage phasor of generator i, denoted by

$$\boldsymbol{E}_i = E_i(\cos\delta_i + \mathbf{i}\sin\delta_i).$$

The magnitude E_i is considered to be a constant following the assumption about classical models. Let the set of generators to which the ith generator is connected be denoted as $\mathcal{N}_i$. We then rewrite (4) as

$$P_{gi} = \sum_{j \in \mathcal{N}_i} \mathrm{Re}\left(\boldsymbol{E}_i \boldsymbol{I}_{ij}^*\right) \tag{5}$$

where $\boldsymbol{I}_{ij} \in \mathbb{C}$ is the current phasor flowing from generator i to generator j. After a few calculations, this simply reduces to

$$P_{gi} = \sum_{j \in \mathcal{N}_i} k_{ij} \sin\left(\delta_i - \delta_j\right) \tag{6}$$

where $k_{ij} := E_i E_j / \chi_{ij}$ is a scalar weight given by χ_{ij} being the reactance (per unit) of the transmission line connecting generators i and j, neglecting the resistance of the line. The simplest state-space form of the swing equations of the ith generator can then be written as

$$\begin{aligned} \dot{\delta}_i &= \omega_i \\ M_i \dot{\omega}_i &= P_{mi} - d_i \omega_i - \sum_{j \in \mathcal{N}_i} k_{ij} \sin\left(\delta_i - \delta_j\right) \end{aligned} \tag{7}$$

for $i = 1, \ldots, n$. Note that the right-hand side of (7) captures the topology of the network, i.e., which generator is connected to which other generators. Depending on the topology, i.e., both the combinatorial structure of $\mathcal{N}_i$ and the weights k_{ij}, the corresponding dynamics of different grid

models will be different. Also note that for deriving (7), we assumed the power to be flowing from generator i to generator j. This means that the ith synchronous machine in this case is acting like a generator while the jth machine is acting like a motor. This assumption is not necessary, and can be easily foregone by defining the following sign convention.

- If power is flowing out of the ith machine and into the jth machine, then this power will have a negative sign in the right-hand side of the swing equation of the ith machine, and positive sign in that of the jth machine. In this case, the ith machine will be in "generation" mode and the jth machine will be in "motor" mode in terms of this power flow.
- Similarly, if power is flowing into the ith machine and out of the jth machine, then this power will have a negative sign in the right-hand side of the swing equation of the jth machine and positive sign in that of the ith machine. In this case, the jth machine will be in "generation" mode and the ith machine will be in "motor" mode in terms of this power flow.

This sign convention easily leads to the following observations.

O1) The effective sign of δ_i on the right-hand side of the ith swing equation is always negative. The word "effective" here accommodates for the fact that sin is an odd function.
O2) Swing equations are direction independent.
O3) Only the neighbors of the ith generator appear in the right-hand side of its swing equation.

We cite an example to make these observations clearer. Consider a system with five generators, as shown in Fig. 3. Consider two different sets of directions for the power flows, as shown in Fig. 3(a) and (b). Following the sign convention, the swing equation for generator 1 in Fig. 3(a), ignoring damping, can be written as

$$M_1\ddot{\delta}_1 = P_{m1} - k_{12}\sin(\delta_1 - \delta_2) - k_{13}\sin(\delta_1 - \delta_3) - k_{14}\sin(\delta_1 - \delta_4). \quad (8a)$$

Following the same sign convention, the swing equation for generation 1 in Fig. 3(b) can be written as

$$M_1\ddot{\delta}_1 = P_{m1} - k_{21}\sin(\delta_2 - \delta_1) - k_{31}\sin(\delta_3 - \delta_1) - k_{14}\sin(\delta_1 - \delta_4). \quad (8b)$$

However, since $k_{ij} = k_{ji}$, and sin is an odd function, we see that (8b) is exactly the same as (8a). Similarly, the swing equation for generator 2 in Fig. 3(a) can be written as

$$M_2\ddot{\delta}_2 = P_{m2} + k_{12}\sin(\delta_1 - \delta_2) \quad (9a)$$

while that for generator 2 in Fig. 3(b) can be written as

$$M_2\ddot{\delta}_2 = P_{m2} - k_{21}\sin(\delta_2 - \delta_1). \quad (9b)$$

Again, (9a) and (9b) are identical. This justifies observation O2), indicating that swing equations are independent of the directions of power flow. Observation O1) is also quite clear

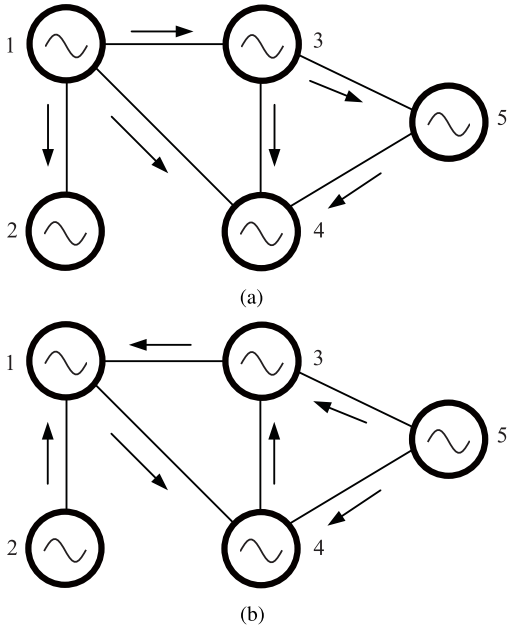

Fig. 3. ***Five-machine power system with different power flow directions. (a) System with five generators, power flow set 1. (b) System with five generators, power flow set 2.***

from the right-hand side of (8a)–(8b). Equation (8a)–(8b), for example, is the swing equation for generator 1, and the effective signs of the angle of generator 1, i.e., δ_1, in every term on the right-hand side of this equation are negative. Similarly, (9a)–(9b) is the swing equation for generator 2, and the effective signs of the angle of generator 2, i.e., δ_2, in every term on the right-hand side of this equation are also negative. All of these observations will become useful when we derive the small-signal model of (7) shortly. As mentioned before, some of the synchronous machines in this system are serving as generators or power producers while some are serving as motors or power consumers. These motors model the loads in the system. The total power thus remains conserved within the system, shuffling from one machine to another. This motion manifests itself in the form of second-order nonlinear oscillations in the phase and frequency of the generators.

For example, for the 10-generator model in Fig. 2(c), we assume $\chi_{1j} = 0.1$ pu for all $j = 2, 3, 4, 5$, $\chi_{6k} = 0.2$ pu for all $k = 7, 8, 9, 10$, and $\chi_{16} = 5$. This results in a two-area system where oscillators 1–5 belong to one area with small transmission line reactances, and oscillators 6–10 belong to another area, also with small line reactances, while the reactance between the central nodes, i.e., nodes 1 and 6, is significantly larger indicating that the two areas are physically distant from each other. Simulating this model, we get the solutions of the frequencies in the two areas as in Fig. 4(a) and (b). It is clear that the local groups of generators in each area synchronize with each other over time. The average motion of the frequencies in area 1 is compared with that in area 2 in Fig. 4(c). This figure shows that the two areas

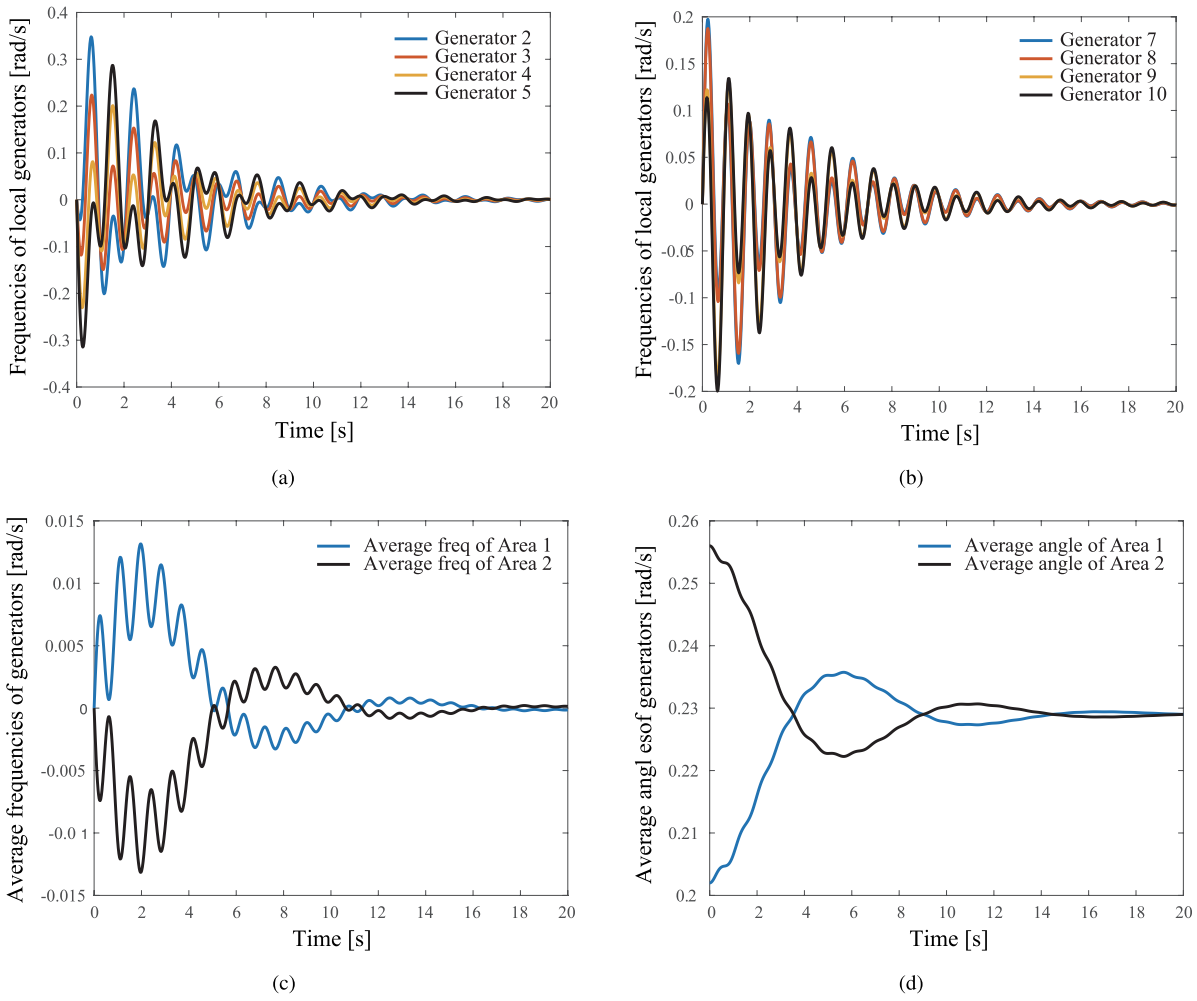

Fig. 4. ***Angle and frequency responses of ten-machine nonlinear swing model. (a) Frequencies of generators in area 1. (b) Frequencies of generators in area 2. (c) Average frequencies of areas 1 and 2. (d) Average angles of areas 1 and 2.***

by themselves are oscillating against each other. A similar behavior is shown for the average of the phase angles, as shown in Fig. 4(d). A somewhat bimodal behavior is visible in the average frequency oscillations. This behavior actually arises from the fact that the reactance between generators 1 and 6 is larger than the reactances between the local generators inside each area. This is a well-known phenomenon in power systems, known as coherency which arises predominantly because of the underlying graph-theoretic properties of the network. We will discuss this property in more details in Section V. Fig. 5 shows the coherency behavior for a 48-machine 140-bus power system model, also popularly known as the Northeastern Power Coordinating Council (NPCC) model [24]. This model very closely represents the power grid of the Northeastern United States. It is divided into nine coherent areas as shown in Fig. 5(a). Fig. 5(b) shows the frequencies of all generators in area 1 and area 6, while Fig. 5(c) shows those for all generators in area 4 and area 8. The out-of-phase behavior is noticeable in both figures. Fig. 5(d) shows the average motions of the frequencies in areas 1 and 6, while Fig. 5(e) shows those for areas 4 and 8. Again, from these figures, one can see that the respective areas are oscillating against each other.

III. NONLINEAR ELECTRICAL MODELS OF POWER SYSTEMS

A. Differential-Algebraic Equation Model

In practice, generators in a power grid are not always directly connected to each other as in the mass-spring-damper model of Section III. They are instead connected through additional electrical points or buses, where no dynamic element may be present and only algebraic power balance holds. An example of this architecture is shown in Fig. 6 for a power system with four generators and six buses. As a result of this structure, the swing equations can no

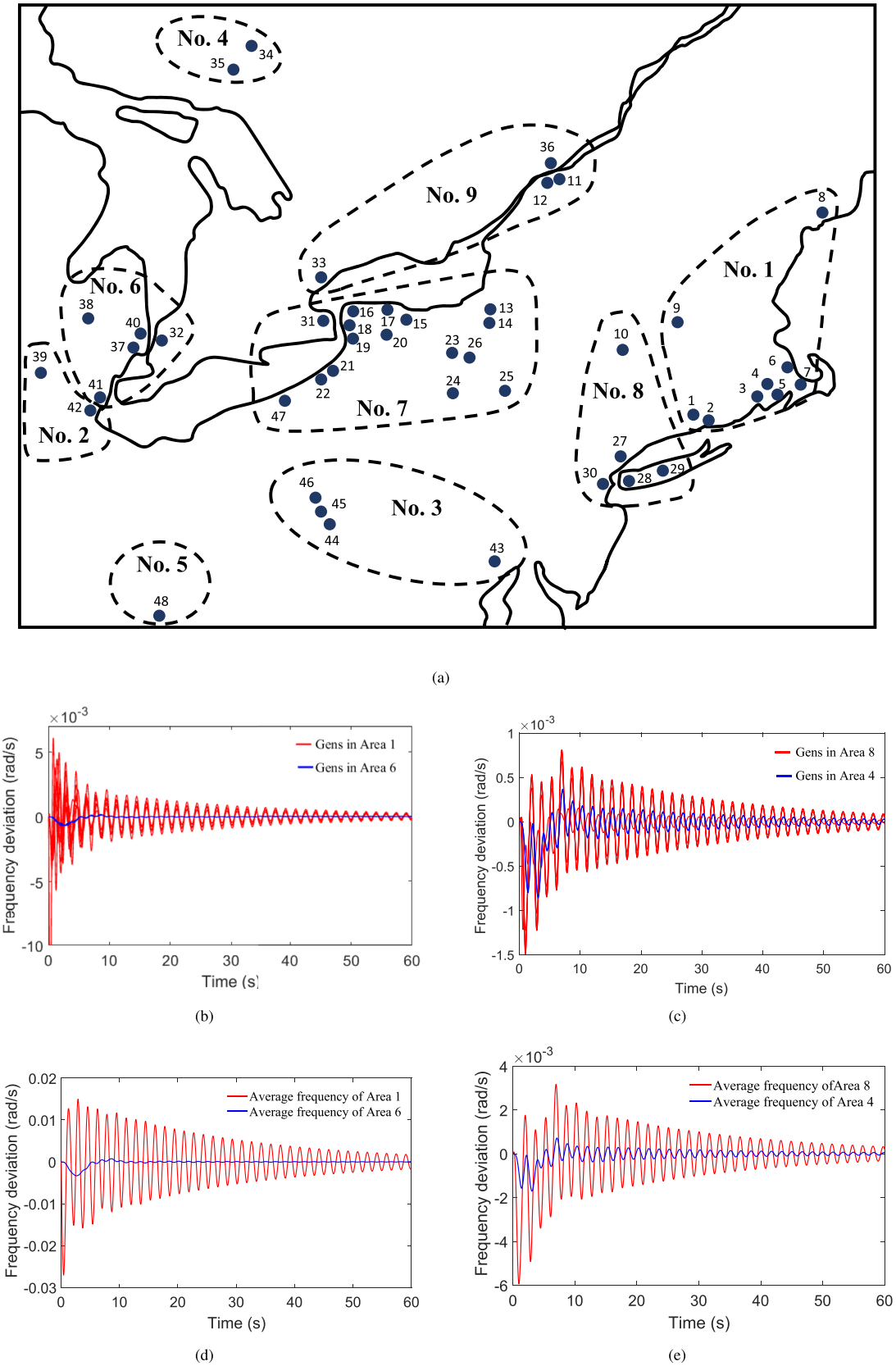

Fig. 5. ***Small-signal frequency responses of 9-area NPCC power system. (a) The NPCC power system with nine coherent clusters. (b) Frequencies of generators in areas 1 and 6. (c) Frequencies of generators in areas 4 and 8. (d) Average frequencies of areas 1 and 6. (e) Average angles of areas 4 and 8.***

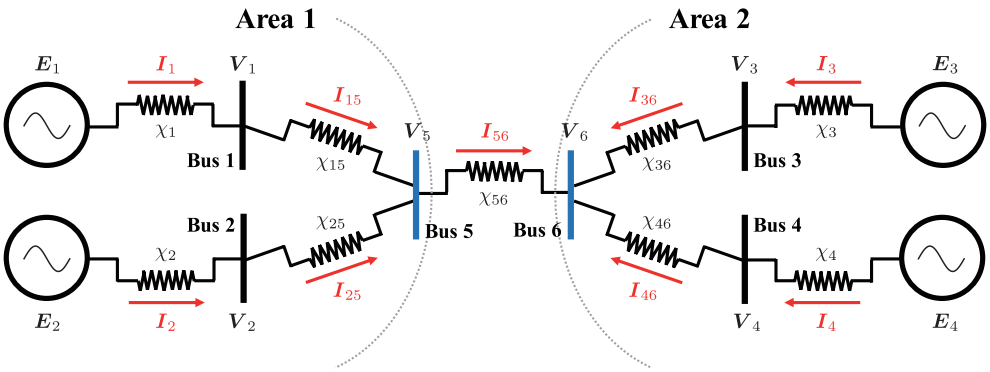

Fig. 6. ***Example of a power network with four generators and two nongenerator buses. The generator buses, i.e., buses 1–4, are denoted by the black bars, and nongenerator buses, i.e., buses 5 and 6, are denoted by the blue bars. The intention behind the area partitioning will be made clear in Section V.***

longer be written directly as ordinary differential equations, but rather have to be expressed in the form of differential-algebraic equations (DAEs).

Fortunately, the DAE can be reduced to an equivalent differential equation albeit at the cost of changing the equivalent topology of the network. In this section, we will explain the construction of the DAE model from physical principles using observations from this simple example. It will be found that a weighted graph Laplacian structure naturally arises in the algebraic equation as reflecting Kirchhoff's current law. We assume the transmission lines to be lossless. We also assume that the model does not have any extraneous load, which in this case means that some of the synchronous machines are operating as generators while the rest are operating as motors or loads. If the model contains additional loads such as constant power/impedance/current loads, then the rows of the network admittance matrix will no longer sum to zero [23].

Let $\mathcal{G}$ and $\overline{\mathcal{G}}$, respectively, denote the label sets for generator and nongenerator buses. Let the numbers of generator and nongenerator buses be denoted by $n := |\mathcal{G}|$ and $\overline{n} := |\overline{\mathcal{G}}|$, respectively. Furthermore, let $\mathcal{E}$ denotes the edge set of the network. This set is undirected, i.e., if $(i,j) \in \mathcal{E}$, then $(j,i) \in \mathcal{E}$, and *vice versa*. For the example in Fig. 6, we see that $\mathcal{G} = \{1,2,3,4\}$, $\overline{\mathcal{G}} = \{5,6\}$, $n = 4$, $\overline{n} = 2$, and

$$\mathcal{E} = \left\{ \begin{matrix} (1,5), & (2,5), & (3,6), & (4,6), & (5,6) \\ (5,1), & (5,2), & (6,3), & (6,4), & (6,5) \end{matrix} \right\}.$$

For each $i \in \mathcal{G} \cup \overline{\mathcal{G}}$, let $\boldsymbol{V}_i \in \mathbb{C}$ denote the complex voltage phasor of the ith bus. For $i \in \mathcal{G}$, let $\boldsymbol{E}_i \in \mathbb{C}$ denote the complex voltage phasor of the ith generator (the magnitude of which is assumed to be constant following the classical model assumption made in Section III), and let $\boldsymbol{I}_i \in \mathbb{C}$ denote the complex current phasor flowing from the internal circuit of the ith generator to the ith generator bus. Then, the generator current and generator bus voltage phasors are related as

$$\boldsymbol{I}_i = \frac{1}{\mathbf{i}\chi_i}(\boldsymbol{E}_i - \boldsymbol{V}_i), \quad i \in \mathcal{G} \tag{10a}$$

where $\chi_i > 0$ denotes the internal reactance of the ith generator. Similarly, the current phasor $\boldsymbol{I}_{ij} \in \mathbb{C}$ flowing from the ith bus to the jth bus can be written as

$$\boldsymbol{I}_{ij} = \frac{1}{\mathbf{i}\chi_{ij}}(\boldsymbol{V}_i - \boldsymbol{V}_j), \quad (i,j) \in \mathcal{E} \tag{10b}$$

where $\chi_{ij} = \chi_{ji} > 0$ denotes the reactance between the ith and jth buses. See the arrows in Fig. 6 for the depiction of current flows.

Let $\mathcal{N}_i$ denote the label set of the neighboring buses of the ith bus, i.e., $\mathcal{N}_i := \{j : (i,j) \in \mathcal{E}\}$. From Kirchhoff's current law it follows that

$$\boldsymbol{I}_i + \sum_{j \in \mathcal{N}_i} \boldsymbol{I}_{ji} = 0, \quad i \in \mathcal{G} \tag{11a}$$

for the ith generator bus, and

$$\sum_{j \in \mathcal{N}_i} \boldsymbol{I}_{ji} = 0, \quad i \in \overline{\mathcal{G}} \tag{11b}$$

for the ith nongenerator bus. For example, at bus 1 in Fig. 6, we have $\boldsymbol{I}_1 + \boldsymbol{I}_{51} = 0$, where $\boldsymbol{I}_{51} = -\boldsymbol{I}_{15}$, and at bus 5, we have $\boldsymbol{I}_{15} + \boldsymbol{I}_{25} + \boldsymbol{I}_{65} = 0$, where $\boldsymbol{I}_{65} = -\boldsymbol{I}_{56}$.

Next, we represent the equalities (10a)–(10b) and (11a)–(11b) in a compact matrix form. To this end, we define the following stacked vectors:

$$\boldsymbol{E}_{\mathcal{G}} := (\boldsymbol{E}_i)_{i \in \mathcal{G}}, \quad \boldsymbol{V}_{\mathcal{G}} := (\boldsymbol{V}_i)_{i \in \mathcal{G}}, \quad \boldsymbol{V}_{\overline{\mathcal{G}}} := (\boldsymbol{V}_i)_{i \in \overline{\mathcal{G}}}.$$

Then, substituting $\boldsymbol{I}_i$ and $\boldsymbol{I}_{ij}$ in (10a)–(10b) into (11a)–(11b), we have the complex-valued algebraic equation

$$\begin{bmatrix} L_{\mathrm{D}} + L_{11} & L_{12} \\ L_{12}^{\mathsf{T}} & L_{22} \end{bmatrix} \begin{bmatrix} \boldsymbol{V}_{\mathcal{G}} \\ \boldsymbol{V}_{\overline{\mathcal{G}}} \end{bmatrix} = \begin{bmatrix} L_{\mathrm{D}} \boldsymbol{E}_{\mathcal{G}} \\ 0 \end{bmatrix} \tag{12}$$

where $L_{\mathrm{D}} := \mathrm{diag}(1/\chi_i)_{i \in \mathcal{G}}$ and

$$L := \begin{bmatrix} L_{11} & L_{12} \\ L_{12}^{\mathsf{T}} & L_{22} \end{bmatrix}. \tag{13}$$

Note that the reciprocals of the imaginary units in (10a)–(10b) are cancelled out by division. Furthermore, L is

$$L = \left[\begin{array}{cccc|cc} 1/\chi_{15} & 0 & 0 & 0 & -1/\chi_{15} & 0 \\ 0 & 1/\chi_{25} & 0 & 0 & -1/\chi_{25} & 0 \\ 0 & 0 & 1/\chi_{36} & 0 & 0 & -1/\chi_{36} \\ 0 & 0 & 0 & 1/\chi_{46} & 0 & -1/\chi_{46} \\ \hline -1/\chi_{15} & -1/\chi_{25} & 0 & 0 & 1/\chi_{15}+1/\chi_{25}+1/\chi_{56} & -1/\chi_{56} \\ 0 & 0 & -1/\chi_{36} & -1/\chi_{46} & -1/\chi_{56} & 1/\chi_{36}+1/\chi_{46}+1/\chi_{56} \end{array}\right]. \tag{14}$$

a weighted graph Laplacian associated with the bus network, the (i,j)-element of which is given as

$$L_{ij} = \begin{cases} \sum_{k\in\mathcal{N}_i} 1/\chi_{ik} & i = j \\ -1/\chi_{ij}, & j \in \mathcal{N}_i \\ 0, & \text{otherwise.} \end{cases}$$

The weighted graph Laplacian for network in Fig. 6 is shown in (14), at the top of this page. As seen from this example, L_{11} is a positive diagonal matrix when every generator bus is indirectly connected to other generator buses.

We next write the complex voltage phasors $\boldsymbol{E}_i$ and $\boldsymbol{V}_i$ in the polar form as

$$\boldsymbol{E}_i := E_i(\cos\delta_i + \mathbf{i}\sin\delta_i), \quad \boldsymbol{V}_i := V_i(\cos\theta_i + \mathbf{i}\sin\theta_i)$$

where $E_i \in \mathbb{R}_{\geq 0}$, $V_i \in \mathbb{R}_{\geq 0}$, $\delta_i \in \mathbb{S}$, and $\theta_i \in \mathbb{S}$. Then, following (7), the dynamics of the ith generator can be written as

$$M_i\ddot{\delta}_i + d_i\dot{\delta}_i = P_{mi} - \frac{E_iV_i}{\chi_i}\sin(\delta_i - \theta_i), \qquad i \in \mathcal{G}. \tag{15}$$

Defining stacked variables

$$E := (E_i)_{i\in\mathcal{G}}, \quad V_{\mathcal{G}} := (V_i)_{i\in\mathcal{G}}, \quad V_{\overline{\mathcal{G}}} := (V_i)_{i\in\overline{\mathcal{G}}}$$
$$\delta := (\delta_i)_{i\in\mathcal{G}}, \quad \theta_{\mathcal{G}} := (\theta_i)_{i\in\mathcal{G}}, \quad \theta_{\overline{\mathcal{G}}} := (\theta_i)_{i\in\overline{\mathcal{G}}}$$

and the stacked constants

$$P_m := (P_{mi})_{i\in\mathcal{G}}, \quad M := \mathrm{diag}\,(M_i)_{i\in\mathcal{G}}, \quad D := \mathrm{diag}\,(d_i)_{i\in\mathcal{G}}$$

we obtain the system of the differential equations

$$M\ddot{\delta} + D\dot{\delta} = P_m - L_{\mathrm{D}}E \circ V_{\mathcal{G}} \circ \mathbf{sin}(\delta - \theta_{\mathcal{G}}) \tag{16a}$$

and the real-valued algebraic equations

$$\begin{bmatrix} L_{\mathrm{D}}+L_{11} & L_{12} \\ L_{12}^{\top} & L_{22} \end{bmatrix}\begin{bmatrix} V_{\mathcal{G}} \circ \mathbf{cos}\,\theta_{\mathcal{G}} \\ V_{\overline{\mathcal{G}}} \circ \mathbf{cos}\,\theta_{\overline{\mathcal{G}}} \end{bmatrix} = \begin{bmatrix} L_{\mathrm{D}}E \circ \mathbf{cos}\delta \\ 0 \end{bmatrix}$$
$$\begin{bmatrix} L_{\mathrm{D}}+L_{11} & L_{12} \\ L_{12}^{\top} & L_{22} \end{bmatrix}\begin{bmatrix} V_{\mathcal{G}} \circ \mathbf{sin}\,\theta_{\mathcal{G}} \\ V_{\overline{\mathcal{G}}} \circ \mathbf{sin}\,\theta_{\overline{\mathcal{G}}} \end{bmatrix} = \begin{bmatrix} L_{\mathrm{D}}E \circ \mathbf{sin}\delta \\ 0 \end{bmatrix}. \tag{16b}$$

The two equations in (16b) correspond to the real and imaginary parts of (12). In fact, (16a)–(16b) represents the DAE form of the swing equations. In Section III-B, we derive how this DAE model can be converted into an equivalent differential equation model by a process referred to as the Kron reduction [25].

B. Kron Reduction

It can be seen from (16b) that the voltage magnitude and angle $(V_{\overline{\mathcal{G}}}, \theta_{\overline{\mathcal{G}}})$ at the nongenerator buses can be represented as the function of $(V_{\mathcal{G}}, \theta_{\mathcal{G}})$ at the generator buses as

$$\begin{aligned} V_{\overline{\mathcal{G}}} \circ \mathbf{cos}\,\theta_{\overline{\mathcal{G}}} &= -L_{22}^{-1}L_{12}^{\top}(V_{\mathcal{G}} \circ \mathbf{cos}\,\theta_{\mathcal{G}}), \\ V_{\overline{\mathcal{G}}} \circ \mathbf{sin}\,\theta_{\overline{\mathcal{G}}} &= -L_{22}^{-1}L_{12}^{\top}(V_{\mathcal{G}} \circ \mathbf{sin}\,\theta_{\mathcal{G}}). \end{aligned} \tag{17a}$$

Note that L_{22} is nonsingular because every principal submatrix of a weighted graph Laplacian, which is a singular M-matrix, is a nonsingular M-matrix (see Fact 4.11.12 (vi) in [26]).

In a similar way, $(V_{\mathcal{G}}, \theta_{\mathcal{G}})$ can be represented as the function of the generator angle δ as

$$\begin{aligned} V_{\mathcal{G}} \circ \mathbf{cos}\,\theta_{\mathcal{G}} &= X(E \circ \mathbf{cos}\delta) \\ V_{\mathcal{G}} \circ \mathbf{sin}\,\theta_{\mathcal{G}} &= X(E \circ \mathbf{sin}\delta) \end{aligned} \tag{17b}$$

where X is a square matrix defined by

$$X := \left(L_{\mathrm{D}} + L_{11} - L_{12}L_{22}^{-1}L_{12}^{\top}\right)^{-1}L_{\mathrm{D}}. \tag{18}$$

Using the trigonometric identity

$$\mathbf{sin}(\delta - \theta_{\mathcal{G}}) = \mathbf{sin}\delta \circ \mathbf{cos}\,\theta_{\mathcal{G}} - \mathbf{cos}\delta \circ \mathbf{sin}\,\theta_{\mathcal{G}}$$

together with (17b), the last term in (16a) can be written as

$$\begin{aligned} &L_{\mathrm{D}}E \circ V_{\mathcal{G}} \circ \mathbf{sin}(\delta - \theta_{\mathcal{G}}) \\ &\quad = E \circ \mathbf{sin}\,\delta \circ (\Gamma(E \circ \mathbf{cos}\,\delta)) - E \circ \mathbf{cos}\,\delta \circ (\Gamma(E \circ \mathbf{sin}\,\delta)) \end{aligned} \tag{19}$$

where Γ is the positive–definite matrix defined by

$$\Gamma := L_{\mathrm{D}}\left(L_{\mathrm{D}} + L_{11} - L_{12}L_{22}^{-1}L_{12}^{\top}\right)^{-1}L_{\mathrm{D}}. \tag{20}$$

Then, applying the identity

$$\sin\delta_i\cos\delta_j - \cos\delta_i\sin\delta_j = \sin(\delta_i - \delta_j)$$

to each element of (19), the Kron-reduced model of (16a)–(16b) is obtained as

$$M_i\ddot{\delta}_i + d_i\dot{\delta}_i = P_{mi} - \sum_{j=1}^{n}\frac{E_iE_j}{\gamma_{ij}}\sin(\delta_i - \delta_j), \quad i \in \mathcal{G} \tag{21}$$

where γ_{ij}, which is equal to γ_{ji}, denotes the inverse of the (i,j)-element of Γ. This equation is similar to the swing equation (7), but there is an important distinction between the

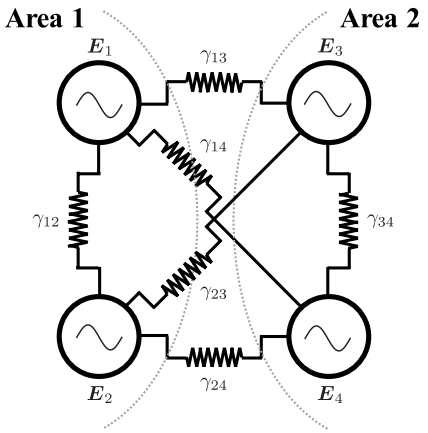

Fig. 7. *The Kron-reduced model of the power network example in Fig. 6. All nongenerator buses are eliminated to derive an equivalent topology where all generators are connected directly to each other.*

two; both X in (18) and Γ in (20) are positive dense matrices, i.e., every element of X and Γ are positive. This will always be true if the weighted graph Laplacian L defined in (13) is irreducible, i.e., if the power network is connected. This is proven as follows. From the formula of the inverse of partitioned matrices (see Fact 2.17.3 in [26]), we see that

$$X = [I_n \quad 0] \begin{bmatrix} L_{\mathrm{D}} + L_{11} & L_{12} \\ L_{12}^{\mathsf{T}} & L_{22} \end{bmatrix}^{-1} \begin{bmatrix} L_{\mathrm{D}} \\ 0 \end{bmatrix}, \quad \Gamma = L_{\mathrm{D}} X.$$

Note that the partitioned matrix to be inverted is irreducible and positive definite. As shown in [27, Th. 5.12], every element of the inverse of an irreducible nonsingular M-matrix is positive. Thus, both X and Γ are shown to be positive dense matrices, because L_{D} is a diagonal matrix having positive diagonal elements. This fact implies that in the Kron-reduced model (21) every generator will be connected to every other generator, and thereby the original network structure will typically be lost.

For example, the original network structure in Fig. 6 is sparse, but its Kron-reduced model as shown in Fig. 7 becomes dense. The two models (16a)–(16b) and (21) are, however, equivalent to each other in the sense that the dynamical behavior of the generator states $\delta(t)$ and $\omega(t)$ in both will be identical. From (16a)–(16b) and (21), it is also straightforward to derive that if the original network did have some generator pairs that are directly connected to each other without any intermediate bus junctions, then the topology between these pairs will remain intact in the Kron-reduced model. In other words, these generators will not be connected to every other generator, but only to the ones that they were directly connected to. This scenario is shown in Figs. 8 and 9.

C. Frequency-Synchronized Solution and Its Stability

We next review several results on frequency synchronization and phase cohesiveness of the Kron-reduced model (21), which have been reported in [16], [28], and [29] to analyze a synchronization property of coupled oscillators evolving over a network. The review presented in the rest of this section can be understood as the equilibrium (steady-state) analysis of the DAE model (16a)–(16b), giving a foundation for linearization analysis in Section IV and transient-state analysis in Section V.

Let $\delta^\star$ be an equilibrium of (21), and $\left(V_{\mathcal{G}}^\star, \theta_{\mathcal{G}}^\star\right)$ and $\left(V_{\mathcal{G}}^\star, \theta_{\mathcal{G}}^\star\right)$ be the corresponding equilibria of the bus voltage variables. The latter are uniquely determined such that

$$\begin{aligned} V_{\mathcal{G}}^\star \circ \mathbf{cos}\, \theta_{\mathcal{G}}^\star &= -L_{22}^{-1} L_{12}^{\mathsf{T}} \left(V_{\mathcal{G}}^\star \circ \mathbf{cos}\, \theta_{\mathcal{G}}^\star\right) \\ V_{\mathcal{G}}^\star \circ \mathbf{sin}\, \theta_{\mathcal{G}}^\star &= -L_{22}^{-1} L_{12}^{\mathsf{T}} \left(V_{\mathcal{G}}^\star \circ \mathbf{sin}\, \theta_{\mathcal{G}}^\star\right) \end{aligned} \tag{22a}$$

which follows from (17a), and

$$\begin{aligned} V_{\mathcal{G}}^\star \circ \mathbf{cos}\, \theta_{\mathcal{G}}^\star &= X(E \circ \mathbf{cos}\, \delta^\star) \\ V_{\mathcal{G}}^\star \circ \mathbf{sin}\, \theta_{\mathcal{G}}^\star &= X(E \circ \mathbf{sin}\, \delta^\star) \end{aligned} \tag{22b}$$

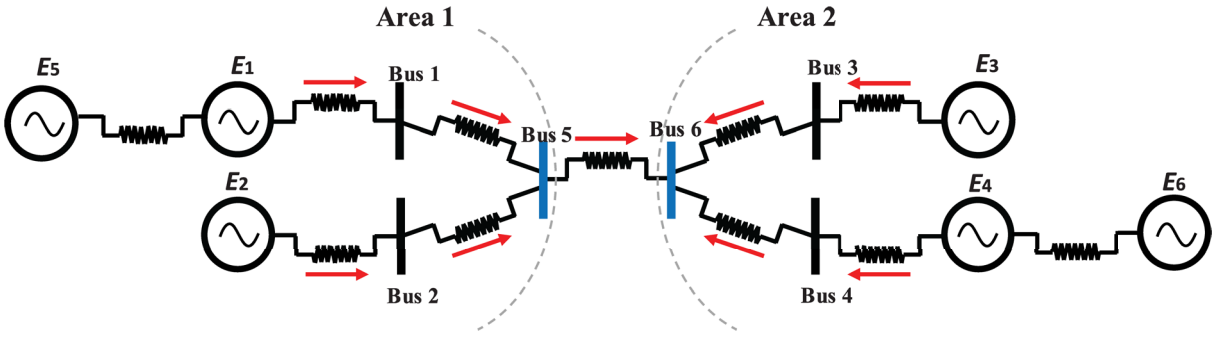

Fig. 8. *Example of a power network with six generators and two nongenerator buses. Generator 5 is directly connected to generator 1, and generator 6 is directly connected to generator 4.*

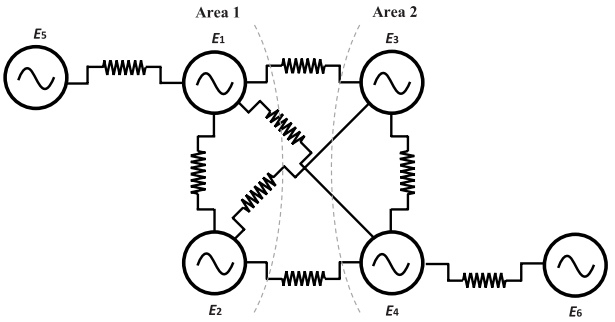

Fig. 9. ***The Kron-reduced model of the power network example in Fig. 8. All nongenerator buses are eliminated by Kron reduction. The connection topology for generator pairs (1,5) and (4,6) remain unchanged.***

which follows from (17b). A comprehensive survey on synchronization of coupled oscillators is given in [16]. Synchronization, in fact, is an extremely important topic for power system stability analysis, especially when the grid is subjected to large-signal disturbances from various causes. This is commonly referred to as transient stability in the power system literature [23]. To understand the impact of network topology on synchronization, we will show that the Jacobian of the nonlinear vector field of the Kron-reduced model (21) is related to the weighted graph Laplacian of its underlying complete graph.

Following the terminology in [16], we say that a solution $\delta : \mathbb{R}_{\geq 0} \to \mathbb{S}^n$ to the differential equation in (21) achieves frequency synchronization if the frequency $\dot{\delta}(t)$ converges to $\omega_{\text{sync}} \mathbb{1}_n$ for a constant frequency ω_{sync} as $t \to \infty$. If a frequency-synchronized solution exists, the synchronization frequency is given as

$$\omega_{\text{sync}} = \frac{\sum_{i=1}^n P_{mi}}{\sum_{i=1}^n d_i}.$$

This can be verified by substituting $\ddot{\delta}_i = 0$ and $\dot{\delta}_i = \omega_{\text{sync}}$ in (21), and by summing the resulting equalities. In this case, a frequency-synchronized solution to (21) is written as

$$\delta_i(t) = \delta_i^\star + \omega_{\text{sync}} t, \quad i \in \mathcal{G} \tag{23}$$

for some constant $\delta_i^\star \in \mathbb{S}$, corresponding to the ith element of $\delta^\star$ in (22b). This means that every generator angle rotates with the identical constant frequency. Transforming the system coordinate to a rotating frame with the frequency ω_{sync} and replacing P_{mi} with $P_{mi} - \omega_{\text{sync}}$, we can always assume that $\omega_{\text{sync}} = 0$, or equivalently $P_m \in \text{im}\, \mathbb{1}_n^\perp$ with $\perp$ indicating the orthogonal subspace, i.e.,

$$P_{m1} + \cdots + P_{mn} = 0$$

without loss of generality. This conclusion is consistent with the observation made in Section III where we implied how some of the synchronous machines in the mass-spring-damper model must serve as generators while the others serve as motors so that the total power in the system is conserved.

Following [16], we say that the frequency-synchronized solution (23) is a phase-cohesive solution to (21) if $|\delta_i^\star - \delta_j^\star| < (\pi/2)$ for every pair $(i,j) \in \mathcal{G} \times \mathcal{G}$. For a compact representation, we represent the phase cohesiveness as $\delta^\star \in \Delta(\pi/2)$, where

$$\Delta\left(\frac{\pi}{2}\right) := \left\{ \delta \in \mathbb{S}^n : |\delta_i - \delta_j| < \frac{\pi}{2}, \forall (i,j) \in \mathcal{G} \times \mathcal{G} \right\}$$

represents the domain of phase cohesive solutions.

The Kron-reduced model (21) can be viewed as an analog of a coupled first-order oscillator model of the form

$$\dot{\delta}_i = P_{mi} - \sum_{j=1}^n \frac{E_i E_j}{\gamma_{ij}} \sin(\delta_i - \delta_j), \quad i \in \mathcal{G} \tag{24}$$

which corresponds to a generalized version of the Kuramoto model [30] where the oscillators are nonuniformly coupled. As stated in [28] and [29], the synchronization properties of (21) and (24) are shown to be equivalent in a reasonable sense. Therefore, we can analyze the frequency-synchronization properties of the Kron-reduced model (21) using the first-order oscillator model (24) instead. Loosely speaking, for a constant $P_m \in \text{im}\, \mathbb{1}_n^\perp$, there exists a locally exponentially stable equilibrium $\delta^\star \in \Delta(\pi/2)$ of (21) if and only if there exists a locally exponentially stable equilibrium $\delta^\star \in \Delta(\pi/2)$ of (24). In particular, if there exists an equilibrium $\delta^\star$, then it must necessarily be located on an equilibrium manifold stemming from the rotational symmetry of the coupling terms. The equilibrium manifold is defined as the following equivalence class [16]:

$$[\delta^\star] := \left\{ \left(\text{rot}_s(\delta_1^\star), \ldots, \text{rot}_s(\delta_n^\star) \right) \in \mathbb{S}^n : s \in [0, 2\pi] \right\} \tag{25}$$

where $\text{rot}_s(\delta) \in \mathbb{S}$ denotes the rotation of δ counterclockwise by the angle s. This is clearly seen from the fact that, for some $\delta^\star$ such that

$$\Psi(\delta^\star) = 0 \tag{26}$$

where $\Psi : \mathbb{S}^n \to \mathbb{R}^n$ denotes the function composed of the right-hand sides of (24) for $i \in \mathcal{G}$, i.e., the ith component of $\Psi(\delta)$ is given by

$$\Psi_i(\delta) = P_{mi} - \sum_{j=1}^n \frac{E_i E_j}{\gamma_{ij}} \sin(\delta_i - \delta_j), \quad i \in \mathcal{G} \tag{27}$$

it follows for any $s \in [0, 2\pi]$ that

$$\Psi\left(\text{rot}_s(\delta_1^\star), \ldots, \text{rot}_s(\delta_n^\star) \right) = 0.$$

Next, we discuss the stability of the equilibrium manifold $[\delta^\star]$. For Ψ in (27), the Jacobian $\partial \Psi / \partial \delta : \mathbb{S}^n \to \mathbb{R}^{n \times n}$ is given by

$$\frac{\partial \Psi_j}{\partial \delta_i}(\delta) = \begin{cases} -\sum_{k=1, k \neq i}^n \frac{E_i E_k}{\gamma_{ik}} \cos(\delta_i - \delta_k), & i = j \\ \frac{E_i E_j}{\gamma_{ij}} \cos(\delta_i - \delta_j), & i \neq j. \end{cases} \tag{28}$$

where $\partial\Psi_j/\partial\delta_i$ denotes the (i,j)-element of $\partial\Psi/\partial\delta$. Because $-\partial\Psi/\partial\delta(\delta)$ is a weighted graph Laplacian for all $\delta \in \Delta(\pi/2)$, the Jacobian evaluated at any equilibrium $\delta^\star \in \Delta(\pi/2)$ is negative semidefinite, and its kernel is $\operatorname{im} \mathbb{1}_n$. Therefore, under a given constant $P_m \in \operatorname{im} \mathbb{1}_n^\perp$, if an equilibrium $\delta^\star \in \Delta(\pi/2)$ exists for (24), or equivalently, if it exists for (21), then the equilibrium manifold $[\delta^\star]$ in (25) is locally exponentially stable. Furthermore, this equilibrium manifold can be uniquely determined in $\Delta(\pi/2)$ (see [29, Lemma 2] for a proof).

D. Existence of Phase Cohesive Solutions

As seen above, the equilibrium manifold $[\delta^\star]$ of phase cohesive solutions is unique in $\Delta(\pi/2)$, and it is locally exponentially stable if a compatible equilibrium $\delta^\star \in \Delta(\pi/2)$ exists. A natural next step, therefore, is to overview results on the existence of equilibria, i.e., the solvability of the nonlinear equation in (26). Generally, both frequency and phase synchronism are related to the graph-theoretic properties of the underlying network such as coupling strength and network homogeneity. In particular, as explained in [16], a weakly coupled and strongly heterogeneous network does not display any coherent behavior, whereas a strongly coupled and sufficiently homogeneous network displays coherent behavior.

The simplest case is when $P_m = 0$. In fact, as shown in [16, Th. 5.1], there exists a phase-synchronized solution to (21) or (24), i.e.,

$$\delta_i^\star = \delta_j^\star \quad \forall (i,j) \in \mathcal{G} \times \mathcal{G} \tag{29}$$

if and only if $P_m = 0$. This result does not depend on the magnitude and homogeneity of the coupling strength $E_i E_j / \gamma_{ij}$. However, in a practical power system, generators (motors) will always be driven by (driving) a mechanical shaft, thereby absorbing (producing) mechanical power. Hence, this scenario, although of theoretical interest, does not hold in practice. A phase-synchronized solution can thus be viewed as an extreme case of phase cohesive solutions.

For a general value of $P_m \in \operatorname{im} 1_n^\perp$, it is not simple to characterize the existence of an equilibrium manifold. One sufficient condition is

$$\lambda_2(\Gamma_0) > \frac{1}{2}\sqrt{\sum_{i,j=1}^{n} (P_{mi} - P_{mj})^2} \tag{30}$$

where $\lambda_2(\Gamma_0)$ denotes the second smallest eigenvalue of the weighted graph Laplacian $\Gamma_0 = -\partial\Psi/\partial\delta(0)$ for the Jacobian given by $\partial\Psi/\partial\delta$ in (28) (see [16, Th. 7.1] for a proof). The magnitude of $\lambda_2(\Gamma_0)$, called algebraic connectivity in graph theory [31], represents how well-connected the oscillators are. It is also relevant to the convergence rate to the equilibrium manifold [32], [33]. The sufficient condition in (30) basically means that a phase cohesive solution exists, i.e., all frequencies synchronize asymptotically, if the coupling strength among oscillators is large enough compared to the degree of the heterogeneity of the input power P_m. Note that Γ_0 is a dense matrix.

Another condition of practical interest is

$$\psi := \Gamma_0^\dagger P_m, \quad |\psi_i - \psi_j| < 1 \quad \forall (i,j) \in \mathcal{G} \times \mathcal{G} \tag{31}$$

where ψ_i denotes the ith element of ψ and $\Gamma_0^\dagger a$ denotes the Moore–Penrose pseudoinverse of Γ_0. Even though this may not work for an arbitrary network, it can provide a sharp condition for phase cohesiveness under particular settings; see [29] for a collection of examples. One particular example shown in [29, Th. 2] is that, for all $P_m \in \Gamma_0 \Omega \subset \operatorname{im} \mathbb{1}_n^\perp$ where

$$\Omega := \{(\omega_i)_{i\in\mathcal{G}} : \omega_i = \Omega_1 \text{ or } \omega_i = \Omega_2, \quad \forall i \in \mathcal{G}\}$$

with some constants Ω_1 and Ω_2, there exists the equilibrium manifold $[\delta^\star] \subset \Delta(\pi/2)$ for (21) or (24) if and only if (31) holds. Furthermore, it follows for $\omega \in \Omega$ that

$$\left|\delta_i^\star - \delta_j^\star\right| = \begin{cases} 0, & \omega_i = \omega_j \\ \arcsin|\Omega_2 - \Omega_1|, & \omega_i \neq \omega_j. \end{cases}$$

This result shows that the partial synchronization of the power network model (16a)–(16b) can be achieved if P_m is given in accordance with a bipolar distribution.

E. Section Summary

In Section III-A, we first derived an electrical model of a power system in the form of a set of nonlinear DAEs. We showed that the weighted graph Laplacian of the underlying network naturally arises in the algebraic equations via Kirchhoff's current law. Thereafter, in Section III-B, we derived an equivalent differential equation model for this DAE using Kron reduction. We found that all generators in the Kron-reduced model are directly connected to each other through equivalent impedances if the original network is connected. Furthermore, based on the fact that the Kron-reduced model can be viewed as an analog to a first-order coupled oscillator model, we have recollected several existing results on the existence and stability of the equilibria for this model in Sections III-C and III-D. The existence of stable equilibria strongly depends on the algebraic connectivity of a weighted graph Laplacian that follows from the Jacobian of the sinusoidal coupling terms in the Kron-reduced model.

IV. LINEARIZATION OF POWER SYSTEM MODELS

A. Kron-Reduced Differential Equation Form

A power grid is always subjected to different types of faults and disturbances causing small changes in its dynamics. Power engineers are, therefore, often interested in analyzing the small-signal behavior of the nonlinear Kron-reduced model (21) in terms of both small-signal stability

and performance. In this section, we derive this model by linearizing (21), and show that it represents second-order consensus dynamics owing to the fact that the Jacobian of the sinusoidal coupling terms is a weighted graph Laplacian.

In the following, we assume that, for a given $P_m \in \operatorname{im} \mathbb{1}_n^{\perp}$, the equilibrium manifold $[\delta^\star] \subset \Delta(\pi/2)$ exists, or equivalently, there exists an equilibrium $\delta^\star \in \Delta(\pi/2)$ such that (26) holds. Linearizing (21) around this equilibrium, we have

$$M\ddot{x} + D\dot{x} - \frac{\partial \Psi}{\partial \delta}(\delta^\star)x = 0 \tag{32}$$

where $(\partial \Psi / \partial \delta)$ is the Jacobian defined as in (28), and $x \in \mathbb{R}^n$ represents the vector of small-signal deviations of the generator phase angles from the equilibrium $\delta^\star$. Note that

$$\frac{\partial \Psi}{\partial \delta}(\delta^\star) = \frac{\partial \Psi}{\partial \delta}\left(\operatorname{rot}_s(\delta_1^\star), \ldots, \operatorname{rot}_s(\delta_n^\star)\right)$$

holds for any $s \in [0, 2\pi]$. This means that we obtain the same linearized Kron-reduced model (32) around any point on the equilibrium manifold $[\delta^\star]$.

Because $-\partial \Psi / \partial \delta(\delta^\star)$ is a weighted graph Laplacian, we see that (32) represents a second-order consensus dynamics such that $\dot{x}(t)$ converges to zero and $x(t)$ converges to $x_{\text{sync}} \mathbb{1}_n$ as $t \to \infty$. The consensus value is calculated as

$$x_{\text{sync}} = \frac{\sum_{i=1}^n d_i x_i(0) + \sum_{i=1}^n M_i \dot{x}_i(0)}{\sum_{i=1}^n d_i}. \tag{33}$$

This is derived as follows. The linearized Kron-reduced model (32) can be written as the first-order form

$$\begin{bmatrix} \dot{x} \\ \ddot{x} \end{bmatrix} = \begin{bmatrix} 0 & I_n \\ M^{-1}\frac{\partial \Psi}{\partial \delta}(\delta^\star) & -M^{-1}D \end{bmatrix} \begin{bmatrix} x \\ \dot{x} \end{bmatrix}.$$

Because $\mathbb{1}_n^\top \partial \Psi / \partial \delta(\delta^\star) = 0$, we see that

$$\begin{bmatrix} \mathbb{1}_n^\top D & \mathbb{1}_n^\top M \end{bmatrix} \begin{bmatrix} \dot{x} \\ \ddot{x} \end{bmatrix} = 0$$

i.e., $\mathbb{1}_n^\top Dx + \mathbb{1}_n^\top M\dot{x}$ is constant. Therefore, we have

$$1_n^\top D\, \mathbb{1}_n x_{\text{sync}} = \mathbb{1}_n^\top Dx(0) + \mathbb{1}_n^\top M\dot{x}(0)$$

which leads to (33); see [34] for convergence rate analysis for a second-order consensus dynamics. This linearized differential equation model can be used to investigate the synchronization of generators for small-signal disturbances. However, the behavior of bus voltage variables, i.e., $(V_{\mathcal{G}}, \theta_{\mathcal{G}})$ and $(V_{\overline{\mathcal{G}}}, \theta_{\overline{\mathcal{G}}})$, is not easy to analyze by this model as the notion of a bus by itself is lost through the Kron reduction. Therefore, in Section IV-B, we consider deriving a linearized differential-algebraic equation model from (16a)–(16b) that explicitly contains the network structure including all buses.

B. Differential-Algebraic Equation Form

Recall the DAE model (16a)–(16b) that consists of swing equations as well as the algebraic power flow equations. For a stable equilibrium $\delta^\star \in \Delta(\pi/2)$ such that (26) holds, let $\left(V_{\mathcal{G}}^\star, \theta_{\mathcal{G}}^\star\right)$ and $\left(V_{\overline{\mathcal{G}}}^\star, \theta_{\overline{\mathcal{G}}}^\star\right)$ be the compatible equilibria for the bus voltage variables such that (22a)–(22b) holds.

Let $z_1 \in \mathbb{R}^{2n}$ be the vector of small-signal deviations of the bus voltage variables from $\left(V_{\mathcal{G}}^\star, \theta_{\mathcal{G}}^\star\right)$, and $z_2 \in \mathbb{R}^{2\overline{n}}$ be the same from $\left(V_{\overline{\mathcal{G}}}^\star, \theta_{\overline{\mathcal{G}}}^\star\right)$. We next linearize the nonlinear DAE model (16a)–(16b) around these equilibria. Introducing the coefficient vectors

$$\begin{aligned} q_i^\dagger &:= \begin{bmatrix} \cos\theta_i^\star & -V_i^\star \sin\theta_i^\star \end{bmatrix} \\ \overline{q}_i^\dagger &:= \begin{bmatrix} \sin\theta_i^\star & V_i^\star \cos\theta_i^\star \end{bmatrix} \end{aligned} \tag{34}$$

we obtain the system of the linear differential equations

$$M\ddot{x} + D\dot{x} + Kx + Fz_1 = 0 \tag{35a}$$

and the linear algebraic equations

$$\begin{bmatrix} Q_{11} & Q_{12} \\ Q_{21} & Q_{22} \end{bmatrix} \begin{bmatrix} z_1 \\ z_2 \end{bmatrix} = \begin{bmatrix} B \\ 0 \end{bmatrix} x \tag{35b}$$

where the system matrices are given by

$$\begin{aligned} K &:= L_{\text{D}} \operatorname{diag}\left(E \circ V_{\mathcal{G}}^\star \circ \cos\left(\delta^\star - \theta_{\mathcal{G}}^\star\right)\right) \\ B &:= \begin{bmatrix} -L_{\text{D}} \operatorname{diag}(E \circ \sin\delta^\star) \\ L_{\text{D}} \operatorname{diag}(E \circ \cos\delta^\star) \end{bmatrix} \\ F &:= L_{\text{D}} \operatorname{diag}\left(\begin{bmatrix} E \circ \sin\left(\delta^\star - \theta_{\mathcal{G}}^\star\right) & -E \circ V_{\mathcal{G}}^\star \circ \cos\left(\delta^\star - \theta_{\mathcal{G}}^\star\right) \end{bmatrix}\right) \end{aligned} \tag{36}$$

and the bus network structure is reflected in

$$\begin{aligned} Q_{11} &:= \begin{bmatrix} (L_{\text{D}} + L_{11}) \operatorname{diag}\left(q_i^\dagger\right)_{i \in \mathcal{G}} \\ (L_{\text{D}} + L_{11}) \operatorname{diag}\left(\overline{q}_i^\dagger\right)_{i \in \mathcal{G}} \end{bmatrix} \\ Q_{12} &:= \begin{bmatrix} L_{12} \operatorname{diag}\left(q_i^\dagger\right)_{i \in \overline{\mathcal{G}}} \\ L_{12} \operatorname{diag}\left(\overline{q}_i^\dagger\right)_{i \in \overline{\mathcal{G}}} \end{bmatrix} \\ Q_{21} &:= \begin{bmatrix} L_{12}^T \operatorname{diag}\left(q_i^\dagger\right)_{i \in \mathcal{G}} \\ L_{12}^T \operatorname{diag}\left(\overline{q}_i^\dagger\right)_{i \in \mathcal{G}} \end{bmatrix} \\ Q_{22} &:= \begin{bmatrix} L_{22} \operatorname{diag}\left(q_i^\dagger\right)_{i \in \overline{\mathcal{G}}} \\ L_{22} \operatorname{diag}\left(\overline{q}_i^\dagger\right)_{i \in \overline{\mathcal{G}}} \end{bmatrix}. \end{aligned}$$

In this linearized model, the generator angle equilibrium $\delta^\star$ as well as the bus voltage equilibria $\left(V_{\mathcal{G}}^\star, \theta_{\mathcal{G}}^\star\right)$ and $\left(V_{\overline{\mathcal{G}}}^\star, \theta_{\overline{\mathcal{G}}}^\star\right)$ are reflected as parameters. However, recall that the bus voltage equilibria are implicit functions of the generator angle equilibrium as shown in (22a)–(22b). This means that $\left(V_{\mathcal{G}}^\star, \theta_{\mathcal{G}}^\star\right)$, and $\left(V_{\overline{\mathcal{G}}}^\star, \theta_{\overline{\mathcal{G}}}^\star\right)$ are not independent parameters. Thus, unless one explicitly uses this relation between $\delta^\star$, $\left(V_{\mathcal{G}}^\star, \theta_{\mathcal{G}}^\star\right)$, and $\left(V_{\overline{\mathcal{G}}}^\star, \theta_{\overline{\mathcal{G}}}^\star\right)$, the linearized DAE model (35a)–(35b) cannot be identified with the linearized Kron-reduced model (32) properly. In the following, we show this identity introducing a particular basis transformation, which makes it easier to utilize the relation in (22a)–(22b).

C. Commutativity of Kron Reduction and Linearization

In this section, we show that a Kron-reduced version of the linearized DAE model coincides with the linearized

version of the nonlinear Kron-reduced model, i.e., the Kron reduction and the linearization are commutative. This commutative property has not been reported in the literature, to the best of the authors' knowledge. To this end, we first consider transforming the linearized DAE model (35a)–(35b) into a tractable form, because (35a)–(35b) involves the equilibria of generator states and bus voltage variables in a complicated fashion. Let us denote the Moore–Penrose pseudoinverses of the coefficient vectors in (34) by

$$q_i := \begin{bmatrix} \cos\theta_i^\star \\ -\frac{1}{V_i^\star}\sin\theta_i^\star \end{bmatrix}, \quad \overline{q}_i := \begin{bmatrix} \sin\theta_i^\star \\ \frac{1}{V_i^\star}\cos\theta_i^\star \end{bmatrix}.$$

Note that these vectors satisfy $q_i q_i^\dagger + \overline{q}_i \overline{q}_i^\dagger = I_2$. Then, with the transformation matrices

$$H_{\mathcal{G}} = \begin{bmatrix} \mathrm{diag}\,(q_i)_{i\in\mathcal{G}} & \mathrm{diag}\,(\overline{q}_i)_{i\in\mathcal{G}} \end{bmatrix}$$
$$H_{\overline{\mathcal{G}}} = \begin{bmatrix} \mathrm{diag}\,(q_i)_{i\in\overline{\mathcal{G}}} & \mathrm{diag}\,(\overline{q}_i)_{i\in\overline{\mathcal{G}}} \end{bmatrix}$$

we consider the basis transformation

$$z_1 = H_{\mathcal{G}}\zeta_1, \quad z_2 = H_{\overline{\mathcal{G}}}\zeta_2 \tag{37}$$

where $\zeta_1 \in \mathbb{R}^{2n}$ and $\zeta_2 \in \mathbb{R}^{2\overline{n}}$ denote the bus voltage variables in the transformed coordinates. Owing to this basis transformation, the algebraic equation in (35a)–(35b) can also be simplified. For example

$$Q_{11} z_1 = (I_2 \otimes (L_{\mathrm{D}} + L_{11}))\,\zeta_1$$

where the right-hand side is composed only of L_D and L_{11}. Furthermore, we see that $FH_{\mathcal{G}} = -B^T$, which simplifies the system representation in the sense that $FH_{\mathcal{G}}$ is dependent on all equilibria $\delta^\star$, $(V_{\mathcal{G}}^\star, \theta_{\mathcal{G}}^\star)$, and $(V_{\overline{\mathcal{G}}}^\star, \theta_{\overline{\mathcal{G}}}^\star)$, while B is dependent on only $\delta^\star$.

Based on this basis transformation, the linear differential equation (35a) can be written as

$$M\ddot{x} + D\dot{x} + Kx - B^\top \zeta_1 = 0 \tag{38a}$$

and the linear algebraic equation (35b) is written as

$$\begin{bmatrix} I_2 \otimes (L_{\mathrm{D}} + L_{11}) & I_2 \otimes L_{12} \\ I_2 \otimes L_{12}^\top & I_2 \otimes L_{22} \end{bmatrix} \begin{bmatrix} \zeta_1 \\ \zeta_2 \end{bmatrix} = \begin{bmatrix} B \\ 0 \end{bmatrix} x. \tag{38b}$$

In this representation, we see that K is dependent on the equilibria $\delta^\star$ and $(V_{\mathcal{G}}^\star, \theta_{\mathcal{G}}^\star)$, B is dependent on just $\delta^\star$, while the other matrices are independent of them. Furthermore, the equilibrium of nongenerator bus voltage variables i.e., $(V_{\overline{\mathcal{G}}}^\star, \theta_{\overline{\mathcal{G}}}^\star)$, no longer appear in the model.

We next apply the Kron reduction to this system by solving the algebraic equations in (38a)–(38b). Note that the realization of the static (algebraic) system in (38a)–(38b) is made symmetric owing to the basis transformation in (37). This enables systematic analysis of its Kron-reduced model as follows. Using

$$T := \begin{bmatrix} -\mathrm{diag}(E \circ \sin\delta^\star) \\ \mathrm{diag}(\mathrm{E} \circ \cos\delta^\star) \end{bmatrix}$$

we have the Kron-reduced model

$$M\ddot{x} + D\dot{x} + (K - G)x = 0 \tag{39}$$

where G is a positive–definite matrix given by

$$G := T^\top \left(I_2 \otimes \begin{bmatrix} L_{\mathrm{D}} & 0 \end{bmatrix} \begin{bmatrix} L_{\mathrm{D}} + L_{11} & L_{12} \\ L_{12}^T & L_{22} \end{bmatrix}^{-1} \begin{bmatrix} L_{\mathrm{D}} \\ 0 \end{bmatrix} \right) T. \tag{40}$$

Note that the positive definiteness of G is made clear owing to the symmetric realization of the static system in (38a)–(38b). Loosely speaking, we can say from this formula that the feedback effect of the static system, composed of the bus network structure, works to decrease the positive definiteness of the coupling matrix among generators. Furthermore, to identify (39) with (32), it suffices to show the identity

$$-\frac{\partial \Psi}{\partial \delta}(\delta^\star) = K(\delta^\star) - G(\delta^\star) \tag{41}$$

where K and G are regarded as functions of $\delta^\star$. In fact, we can verify this identity using the relation of (22b), which works to rewrite the term

$$V_{\mathcal{G}}^\star \circ \mathbf{cos}(\delta^\star - \theta_{\mathcal{G}}^\star) = \mathbf{cos}\,\delta^\star \circ V_{\mathcal{G}}^\star \circ \mathbf{cos}\,\theta_{\mathcal{G}}^\star + \mathbf{sin}\,\delta^\star \circ V_{\mathcal{G}}^\star \circ \mathbf{sin}\,\theta_{\mathcal{G}}^\star$$

involved in K of (36). The weighted graph Laplacian given as the Jacobian $\partial\Psi/\partial\delta$ in (28) can be now represented as the difference of the positive diagonal matrix K and the positive–definite matrix G. This can be understood as the commutative property of the Kron reduction and the linearization.

D. Section Summary

In Section IV-A, we derived a linearized differential equation model by linearizing the Kron-reduced model in Section III-B. The linearized Kron-reduced model has a second-order consensus dynamics whose coupling matrix is given as the Jacobian in Section III-C with a weighted graph Laplacian structure. In Section IV-B, we applied linearization directly to the DAE model from Section III-A that contains the bus network structure. The resulting model involves the equilibria of generator states and bus voltage variables in a complicated fashion, which is then transformed into a tractable form in Section IV-C. This transformation makes it easier to verify that the Kron-reduced version of the linearized DAE model coincides with the linearized version of the nonlinear Kron-reduced model. In other words, the Kron reduction and the linearization are commutative. Generalization of this result to more complicated power network models such as models involving excitation dynamics of the generators (see Section VI) will be an interesting direction for future work.

V. DYNAMICAL PHASE SYNCHRONIZATION ANALYSIS

A. Dynamical Synchronism of Generators and Generator Buses

In this section, we analyze the dynamical behavior of the nonlinear DAE model (16a)–(16b) based on its linearized DAE model (38a)–(38b). In particular, characterizing its

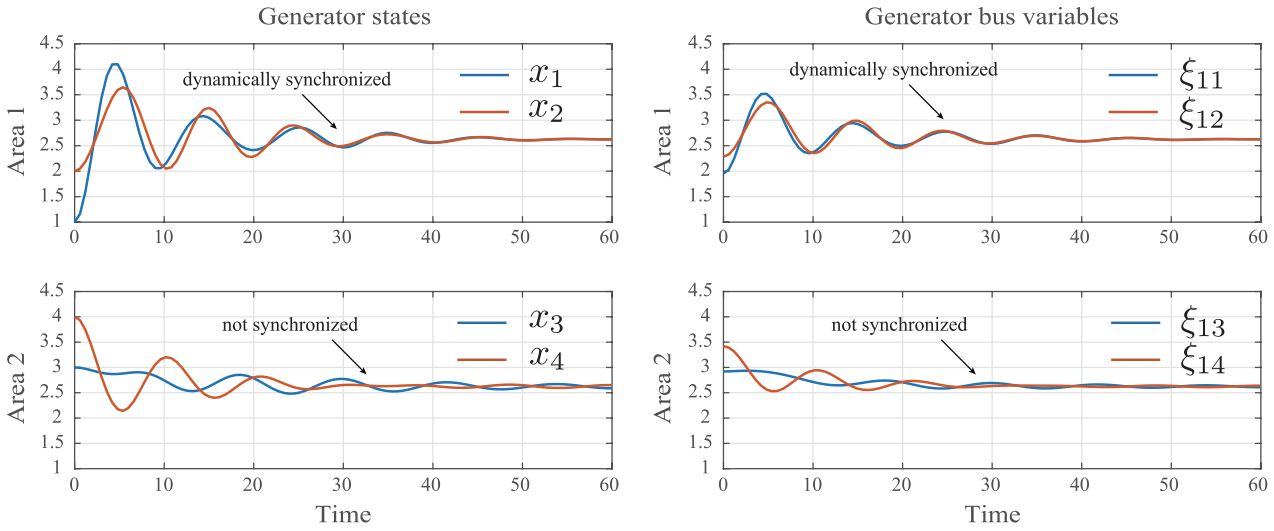

Fig. 10. ***Initial value response of the simplified linear model (42a)–(42b). The system parameters are set as $\chi_1 = \chi_2 = 0.1$, $\chi_3 = 0.1$, $\chi_4 = 0.05$, $\chi_{15} = \chi_{25} = 0.2$, $\chi_{36} = 1$, $\chi_{46} = 0.1$, $\chi_{56} = 0.5$, $M_1 = M_2 = 1$, $d_1 = d_2 = 0.2$, $M_3 = 2$, $M_4 = 3$, $d_3 = 0.1$, and $d_4 = 0.2$. The initial condition is set as $x(0) = (-0.06, 0.19, 0.06, 0.25)$ and $x(0) = 0$.***

dynamic synchronism based on the notion of graph symmetry, we develop an aggregation method for (16a)–(16b) while preserving generator as well as the bus network structures. To the best of the authors' knowledge, this aggregation method has not yet been reported in the literature.

In the following, we suppose that $E_i = 1$ for all $i \in \mathcal{G}$ and the steady state of (16a)–(16b) achieves the phase synchronization of $\delta^\star = 0$, which implies $P_m = 0$. These assumptions are only made hypothetically to simply the derivations; neither of them is essential in the subsequent discussion. For small-signal models, $P_m = 0$ is a standard assumption [23]. Based on this premise, we can further simplify the linearized DAE model (38a)–(38b) as

$$M\ddot{x} + D\dot{x} + Kx - L_{\mathrm{D}}\xi_1 = 0 \tag{42a}$$

with the simplified algebraic equation

$$\begin{bmatrix} L_{\mathrm{D}} + L_{11} & L_{12} \\ L_{12}^{\mathsf{T}} & L_{22} \end{bmatrix} \begin{bmatrix} \xi_1 \\ \xi_2 \end{bmatrix} = \begin{bmatrix} L_{\mathrm{D}} \\ 0 \end{bmatrix} x. \tag{42b}$$

This simplification is made possible because the upper and lower half components of B in (36) become 0 and L_{D}, respectively, which implies that the bus voltage variables $\xi_1 \in \mathbb{R}^n$ and $\xi_2 \in \mathbb{R}^{\overline{n}}$ coincide with the lower half components of $\zeta_1 \in \mathbb{R}^{2n}$ and $\zeta_2 \in \mathbb{R}^{2\overline{n}}$, and their upper half components are identically zero. Furthermore, because G in (40) is reduced to Γ in (20) and $K - G$ is a weighted graph Laplacian, we see that $K = \mathrm{diag}(\Gamma \mathbb{1}_n)$. Thus, the Kron-reduced model of (42a)–(42b) is written as

$$M\ddot{x} + D\dot{x} + (\mathrm{diag}(\Gamma \mathbb{1}_n) - \Gamma)x = 0. \tag{43}$$

As discussed in Section IV-A, the generator state $x(t)$ converges to $x_{\mathrm{sync}} \mathbb{1}_n$ as $t \to \infty$ for x_{sync} in (33). In addition, the generator bus voltage variable $\xi_1(t)$ also converges to the same value because of

$$\xi_1(t) = Xx(t), \quad \forall t \geq 0 \tag{44}$$

where X in (18) satisfies $X\mathbb{1}_n = \mathbb{1}_n$. This property of X is proven by

$$\left(L_{\mathrm{D}} + L_{11} - L_{12}L_{22}^{-1}L_{12}^{\mathsf{T}}\right)\mathbb{1}_n = L_{\mathrm{D}}\mathbb{1}_n$$

which comes from the fact that the Schur complement of the weighted graph Laplacian L in (13) is again a weighted graph Laplacian. In particular, because $L\mathbb{1}_{n+\overline{n}} = 0$ is equivalent to

$$L_{11}\mathbb{1}_n + L_{12}\mathbb{1}_{\overline{n}} = 0, \quad L_{12}^{\mathsf{T}}\mathbb{1}_n + L_{22}\mathbb{1}_{\overline{n}} = 0$$

we can see that $\left(L_{11} - L_{12}L_{22}^{-1}L_{12}^{\mathsf{T}}\right)\mathbb{1}_n = 0$.

To numerically observe the behavior of the simplified linear DAE model (42a)–(42b), we revisit the power network example in Fig. 6. In particular, we consider a situation where generators 1 and 2 in area 1 have the same physical parameters, i.e., $M_1 = M_2$ and $d_1 = d_2$. A similar symmetry is supposed to be inherent in the bus network of area 1, i.e., $\chi_1 = \chi_2$ and $\chi_{15} = \chi_{25}$. In this situation, generators 1 and 2 as well as buses 1 and 2 show some dynamically cohesive and synchronized behavior as can be anticipated from the symmetry (homogeneity) of interaction and the similarity of their physical parameters. In fact, as shown in Fig 10, which shows an initial value response of (42a)–(42b), the disagreement between x_1 and x_2 and that between ξ_{11} and ξ_{12}, denoting the first and second elements of ξ_1, decrease as time goes to infinity, while the disagreement between x_3 and x_4 and that between ξ_{13} and ξ_{14} do not. Furthermore, their

trajectories synchronize even when the system still shows transient behavior. In the following, we analyze this dynamical synchronization of generator states and generator bus voltage variables from a viewpoint of graph symmetry.

B. Analysis Based on Graph Symmetry

Let us denote the subspace of the synchronism between the ith and jth elements of the small-signal state vector $x(t)$ by

$$\mathcal{X}_{ij} := \left\{x \in \mathbb{R}^n : x_i = x_j\right\}. \tag{45}$$

Then, for the simplified linear DAE model (42a)–(42b), we say that the ith and jth generators are dynamically synchronized if

$$x(t) \in \mathcal{X}_{ij}, \quad \forall t \geq 0 \tag{46}$$

for any initial conditions $x(0) \in \mathcal{X}_{ij}$ and $\dot{x}(0) \in \mathcal{X}_{ij}$. Note that (45) is equivalent to

$$x_i(t) = x_j(t), \quad \forall t \geq 0.$$

In a similar manner, we say that the ith and jth generator buses are dynamically synchronized if

$$\xi_1(t) \in \mathcal{X}_{ij} \quad \forall t \geq 0 \tag{47}$$

for any $x(0) \in \mathcal{X}_{ij}$ and $\dot{x}(0) \in \mathcal{X}_{ij}$. Note that the initial condition $\xi_1(0)$ of the bus voltage variables is uniquely determined by the generator state initial condition $x(0)$ due to the relation in (44).

To characterize this dynamical synchronism in an algebraic manner, we define a set of symmetrical matrices with respect to the permutation of the ith and jth columns and rows by

$$\mathcal{S}_{ij} := \left\{A \in \mathbb{R}^{n\times n} : A\Pi_{ij} = \Pi_{ij}A\right\} \tag{48}$$

where Π_{ij} denotes the permutation matrix exchanging the ith and jth elements. Note that $\mathcal{S}_{ij}$ is not the set of usual symmetric (Hermitian) matrices; the condition in (48) represents the invariance with respect to the permutation of the ith and jth columns and rows, i.e., $\Pi_{ij}^{\top} A \Pi_{ij} = A$. For example, we see that the weighted graph Laplacian L in (14) of the bus network in Fig. 6 belongs to $\mathcal{S}_{12}$ if and only if $\chi_{15} = \chi_{25}$, which corresponds to the symmetry of buses 1 and 2. This type of graph symmetry is called graph automorphism in graph theory [35], [36].

Let us first consider characterizing the dynamical synchronism of generator states based on the Kron-reduced model (43). When $M \in \mathcal{S}_{ij}$, meaning $M_i = M_j$, it follows that the ith and jth generators are dynamically synchronized, i.e., (46) holds, if and only if the damping matrix D belongs to $\mathcal{S}_{ij}$, i.e., $d_i = d_j$, and the coupling matrix $\mathrm{diag}(\Gamma \mathbb{1}_n) - \Gamma$ also belongs to $\mathcal{S}_{ij}$, i.e.,

$$\gamma_{ij} = \gamma_{ji}, \quad \gamma_{ik} = \gamma_{jk} \quad \forall k \in \mathcal{G}\backslash\{i,j\}.$$

Note that the relation between the diagonal entries γ_{ii} and γ_{jj} cannot be deduced from this analysis of generator state synchronism, but it can only be deduced from the analysis of the synchronism for the bus voltage variables. In fact, using the relation $\Gamma = L_{\mathrm{D}} X$ and that in (44), it can be shown that the ith and jth generators as well as the ith and jth bus voltage variables are dynamically synchronized, i.e., both (46) and (47) hold, if and only if $\Gamma \in \mathcal{S}_{ij}$. Furthermore, $\Gamma \in \mathcal{S}_{ij}$ is shown to be equivalent to

$$L_{\mathrm{D}} \in \mathcal{S}_{ij}, \quad L_{11} - L_{12}L_{22}^{-1}L_{12}^{\top} \in \mathcal{S}_{ij}. \tag{49}$$

Note that the right condition in (49), which represents the symmetry of a bus network in which the nongenerator buses are Kron reduced, is implied by $L \in \mathcal{S}_{ij}$ for $(i,j) \in \mathcal{G} \times \mathcal{G}$. This represents the symmetry of the whole bus network with respect to the ith and jth generator buses. In conclusion, we see that the symmetry (graph automorphism) of bus networks algebraically characterizes the dynamical synchronism of generator states and the generator bus voltage variables.

C. Application to Generator and Generator Bus Aggregation

Based on the foregoing analysis, we next address the topic of aggregation in power systems. Aggregation, in fact, is a very popular concept for power system models. Given the large size and extraordinary complexity of any realistic power system, deriving and simulating the dynamic model for an entire network such as (42a)–(42b) becomes extremely challenging. Constructing approximate, aggregated, reduced-order models using simplifying assumptions, therefore, becomes almost imperative in practice. The foundations of model aggregation were laid in the late 1970s by Chow and Kokotovic [37], resulting in algorithms of partitioning a power network into dynamic aggregates, where each aggregate consists of a group of strongly connected generators that synchronize over a fast time scale and, thereafter, act as a single entity, while the aggregates themselves are weakly connected to each other, and synchronize over a slower time scale. Their approach was complimented by alternative techniques such as in [38]–[40].

However, these conventional aggregation methods apply aggregation directly on the Kron-reduced model. Very little insights are available currently in understanding how not only generators but also buses can be aggregated so that the reduced-order model retains the concept of a bus. This, in turn, may be necessary for designing shunt controllers that are entirely dependent on the "bus" concept [41].

In this section, we address this problem by deriving a dynamic equivalent model for (42a)–(42b) where aggregation is performed on both generator states and the generator bus voltage variables. In particular, we take an approach based on network clustering. Several clustering algorithms have been reported in recent papers such as [42]–[44].

The results presented here follow the clustering-based model reduction methods developed in, e.g., [45]–[48], which are based on similarity of state trajectories, almost equitable partition of graphs, and passivity of subsystems.

We introduce the notion of network clustering as follows. Let $\hat{\mathcal{G}} := \{1, \ldots, \hat{n}\}$ denote an index set such that $\hat{n} \leq n$. A family of index sets, denoted by $\{\mathcal{I}_l\}_{l \in \hat{\mathcal{G}}}$, is called a cluster set if each element $\mathcal{I}_l$, called a cluster, is a disjoint subset of $\hat{\mathcal{G}}$ and it satisfies $\cup_{l \in \hat{\mathcal{G}}} \mathcal{I}_l = \mathcal{G}$. Furthermore, an aggregation matrix compatible with $\{\mathcal{I}_l\}_{l \in \mathbb{L}}$ is defined by

$$P := \begin{bmatrix} e_{\mathcal{I}_1} \mathbb{1}_{|\mathcal{I}_1|} & \cdots & e_{\mathcal{I}_{\hat{n}}} \mathbb{1}_{|\mathcal{I}_{\hat{n}}|} \end{bmatrix} \in \mathbb{R}^{n \times \hat{n}}. \tag{50}$$

For example, when we consider aggregating the generators and their buses in area 1 of Fig. 6, the cluster set is constructed as

$$\mathcal{I}_1 = \{1, 2\}, \quad \mathcal{I}_2 = \{3\}, \quad \mathcal{I}_3 = \{4\} \tag{51a}$$

for which $\hat{\mathcal{G}} = \{1, 2, 3\}$. In a similar way, when aggregating the generators in both areas 1 and 2, it is constructed as

$$\mathcal{I}_1 = \{1, 2\}, \quad \mathcal{I}_2 = \{3, 4\} \tag{51b}$$

for which $\hat{\mathcal{G}} = \{1, 2\}$. The corresponding aggregation matrices are given as

$$P = \begin{bmatrix} 1 & 0 & 0 \\ 1 & 0 & 0 \\ 0 & 1 & 0 \\ 0 & 0 & 1 \end{bmatrix}, \quad P = \begin{bmatrix} 1 & 0 \\ 1 & 0 \\ 0 & 1 \\ 0 & 1 \end{bmatrix}$$

for (51a) and (51b), respectively.

As seen from the structure of P in (50), the aggregation and the average of a vector $v \in \mathbb{R}^n$ can be represented, respectively, as the $\hat{n}$-dimensional vectors of

$$\hat{v} := P^{\mathsf{T}} v, \quad \mathrm{ave}(v) := P^{\dagger} v$$

where $P^{\dagger}$ denotes the Moore–Penrose pseudoinverse of P. Note that the lth element of $\hat{v}$ is given as $\sum_{i \in \mathcal{I}_l} v_i$. Furthermore, the lth element of $\mathrm{ave}(v)$ is given as $\sum_{i \in \mathcal{I}_l} v_i / |\mathcal{I}_l|$. This is because

$$P^{\dagger} = (P^{\mathsf{T}} P)^{-1} P^{\mathsf{T}}, \quad P^{\mathsf{T}} P = \mathrm{diag}\left(|\mathcal{I}_l|\right)_{l \in \hat{\mathcal{G}}}.$$

Based on these relations, we introduce the aggregated coefficient matrices

$$\hat{M} := P^{\mathsf{T}} M P, \quad \hat{D} := P^{\mathsf{T}} D P, \quad \hat{K} := P^{\mathsf{T}} K P$$

and the aggregated reactance matrices

$$\hat{L}_{\mathrm{D}} := P^{\mathsf{T}} L_{\mathrm{D}} P, \quad \begin{bmatrix} \hat{L}_{11} & \hat{L}_{12} \\ \hat{L}_{12}^{\mathsf{T}} & \hat{L}_{22} \end{bmatrix} := \begin{bmatrix} P^{\mathsf{T}} L_{11} P & P^{\mathsf{T}} L_{12} \\ L_{12}^{\mathsf{T}} P & L_{22} \end{bmatrix}.$$

Using these matrices, we define an aggregated DAE model of (42a)–(42b) by the $\hat{n}$-dimensional differential equation

$$\hat{M} \ddot{\hat{x}} + \hat{D} \dot{\hat{x}} + \hat{K} \hat{x} - \hat{L}_{\mathrm{D}} \hat{\xi}_1 = 0 \tag{52a}$$

and the $(\hat{n} + \overline{n})$-dimensional algebraic equation

$$\begin{bmatrix} \hat{L}_{\mathrm{D}} + \hat{L}_{11} & \hat{L}_{12} \\ \hat{L}_{12}^{\mathsf{T}} & \hat{L}_{22} \end{bmatrix} \begin{bmatrix} \hat{\xi}_1 \\ \hat{\xi}_2 \end{bmatrix} = \begin{bmatrix} \hat{L}_{\mathrm{D}} \\ 0 \end{bmatrix} \hat{x} \tag{52b}$$

whose initial condition is given as

$$\hat{x}(0) = \mathrm{ave}(x(0)), \quad \dot{\hat{x}}(0) = \mathrm{ave}(\dot{x}(0))$$

i.e., the average of the original initial condition. This initial condition satisfies $x(0) = P\hat{x}(0)$ and $\dot{x}(0) = P\dot{\hat{x}}(0)$ if and only if $x(0)$ and $\dot{x}(0)$ lie in the image of P.

Note that the aggregated network (with buses) is represented by the matrix

$$\hat{L} = \begin{bmatrix} \hat{L}_{11} & \hat{L}_{12} \\ \hat{L}_{12}^{\mathsf{T}} & \hat{L}_{22} \end{bmatrix}$$

which is shown to be a weighted graph Laplacian owing to $\mathbb{1}_n = P \mathbb{1}_{\hat{n}}$. A similar projection-based approach for preserving the Laplacian structure of matrices was recently shown in [49]. Furthermore, $\hat{L}_{\mathrm{D}}$ and $\hat{L}_{11}$ are, again, positive diagonal matrices. The preservation of these particular structures can be interpreted as the preservation of physical properties stemming from Kirchhoff's current law as shown in Section III-A. In fact, the aggregated DAE model (52a)–(52b) can be identified with a linearized and simplified model of the aggregated nonlinear DAE model defined as

$$\hat{M} \ddot{\hat{\delta}} + \hat{D} \dot{\hat{\delta}} = \hat{P}_m - \hat{L}_{\mathrm{D}} \hat{E} \circ \hat{V}_{\hat{\mathcal{G}}} \circ \mathbf{sin}(\hat{\delta} - \hat{\theta}_{\hat{\mathcal{G}}}) \tag{53a}$$

with the aggregated algebraic equation

$$\begin{aligned} \begin{bmatrix} \hat{L}_{\mathrm{D}} + \hat{L}_{11} & \hat{L}_{12} \\ \hat{L}_{12}^{\mathsf{T}} & \hat{L}_{22} \end{bmatrix} \begin{bmatrix} \hat{V}_{\hat{\mathcal{G}}} \circ \cos \hat{\theta}_{\hat{\mathcal{G}}} \\ \hat{V}_{\overline{\mathcal{G}}} \circ \cos \hat{\theta}_{\overline{\mathcal{G}}} \end{bmatrix} &= \begin{bmatrix} \hat{L}_{\mathrm{D}} \hat{E} \circ \cos \hat{\delta} \\ 0 \end{bmatrix} \\ \begin{bmatrix} \hat{L}_{\mathrm{D}} + \hat{L}_{11} & \hat{L}_{12} \\ \hat{L}_{12}^{\mathsf{T}} & \hat{L}_{22} \end{bmatrix} \begin{bmatrix} \hat{V}_{\hat{\mathcal{G}}} \circ \sin \hat{\theta}_{\hat{\mathcal{G}}} \\ \hat{V}_{\overline{\mathcal{G}}} \circ \sin \hat{\theta}_{\overline{\mathcal{G}}} \end{bmatrix} &= \begin{bmatrix} \hat{L}_{\mathrm{D}} \hat{E} \circ \sin \hat{\delta} \\ 0 \end{bmatrix} \end{aligned} \tag{53b}$$

where $\hat{\delta}$ denotes the aggregated generator state, $\left(\hat{V}_{\hat{\mathcal{G}}}, \hat{\theta}_{\hat{\mathcal{G}}}\right)$ and $\left(\hat{V}_{\overline{\mathcal{G}}}, \hat{\theta}_{\overline{\mathcal{G}}}\right)$ denote the aggregated generator and the aggregated nongenerator bus voltage variables, and $\hat{P}_m$ and $\hat{E}$ are given as $P^{\mathsf{T}} P_m$ and $\mathrm{ave}(E)$, respectively. The aggregated DAE model of the power network example in Fig. 6 is depicted in Fig. 11, where (a) and (b) correspond to the cluster sets in (51a) and (51b), respectively.

To discuss the dynamical behavior of the aggregated DAE model, let us next define the subspace of synchronism for clusters as

$$\mathcal{X}_{\mathrm{cl}} := \bigcap_{l \in \hat{\mathcal{G}}} \bigcap_{(i,j) \in \mathcal{G}_l \times \mathcal{G}_l} \mathcal{X}_{ij} \tag{54}$$

where $\mathcal{X}_{ij}$ is defined as in (45). Note that $\mathcal{X}_{\mathrm{cl}}$ is identical to $\mathrm{im}\, P$. Furthermore, we define a set of symmetrical matrices corresponding to $\mathcal{X}_{\mathrm{cl}}$ as

$$\mathcal{S}_{\mathrm{cl}} := \bigcap_{l \in \hat{\mathcal{G}}} \bigcap_{(i,j) \in \mathcal{G}_l \times \mathcal{G}_l} \mathcal{S}_{ij}. \tag{55}$$

If all the generators are identical, i.e.,

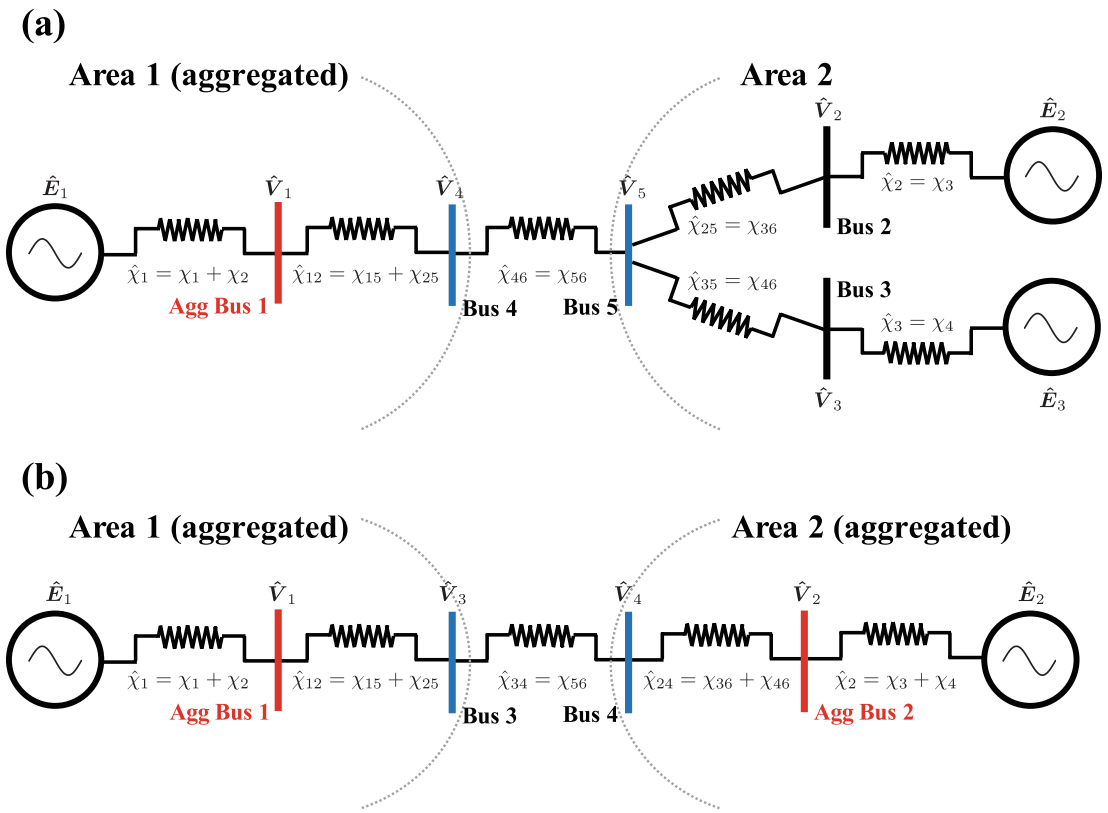

Fig. 11. ***(a) Aggregated model of the power network example in Fig. 6, compatible with the cluster set in (51a). The impedances satisfy $1/\hat{\chi}_1 = 1/\chi_1 + 1/\chi_2$, $1/\hat{\chi}_{12} = 1/\chi_{15} + 1/\chi_{25}$, $1/\hat{\chi}_{46} = 1/\chi_{56}$, $1/\hat{\chi}_{25} = 1/\chi_{36}$, $1/\hat{\chi}_{35} = 1/\chi_{46}$, $1/\hat{\chi}_2 = 1/\chi_3$, and $1/\hat{\chi}_3 = 1/\chi_4$. (b) Aggregated model of the power network example, compatible the cluster set in (51b). The impedances satisfy $1/\hat{\chi}_1 = 1/\chi_1 + 1/\chi_2$, $1/\hat{\chi}_{12} = 1/\chi_{15} + 1/\chi_{25}$, $1/\hat{\chi}_{46} = 1/\chi_{56}$, $1/\hat{\chi}_{24} = 1/\chi_{36} + 1/\chi_{46}$, and $1/\hat{\chi}_2 = 1/\chi_3 + 1/\chi_4$.***

$$M \in \mathcal{S}_{\mathrm{cl}}, \quad D \in \mathcal{S}_{\mathrm{cl}} \tag{56}$$

meaning that $M_i = M_j$ and $d_i = d_j$ for all $(i,j) \in \mathcal{I}_l \times \mathcal{I}_l$ and $l \in \widehat{\mathcal{G}}$, and if

$$L_{\mathrm{D}} \in \mathcal{S}_{\mathrm{cl}}, \quad L_{11} - L_{12} L_{22}^{-1} L_{12}^{\top} \in \mathcal{S}_{\mathrm{cl}} \tag{57}$$

which represents network symmetry compatible with (49), then the simplified linear DAE model (42a)–(42b) and its aggregated DAE model (52a)–(52b) satisfy

$$x(t) = P\hat{x}(t), \quad \xi_1(t) = P\hat{\xi}_1(t), \quad \forall t \geq 0 \tag{58a}$$

for any initial conditions $x(0) \in \mathcal{X}_{\mathrm{cl}}$ and $\dot{x}(0) \in \mathcal{X}_{\mathrm{cl}}$ and, at the same time, they satisfy

$$\hat{x}(t) = \mathrm{ave}(x(t)), \quad \hat{\xi}_1(t) = \mathrm{ave}(\xi_1(t)), \quad \forall t \geq 0 \tag{58b}$$

for any $x(0) \in \mathbb{R}^n$ and $\dot{x}(0) \in \mathbb{R}^n$. In particular, (57) is equivalent to (58a)–(58b) provided that $|\mathcal{I}_l| \leq 2$ for all $l \in \widehat{\mathcal{G}}$ A similar result for systems defined by ordinary differential equations is shown in [50, Th. 4].

We numerically verify the behavior of the aggregated DAE model (52a)–(52b), and compare it with the behavior of the simplified linear DAE model (42a)–(42b). Fig. 12 shows the initial value responses of (42a)–(42b) and (52a)–(52b) when we construct the cluster set as in (51a) following the network structure shown in Fig. 11(a). Because the system parameters (listed in the caption of Fig. 10) actually satisfy the conditions (56) and (57), the behavior of the generator states and generator bus voltage variables of the aggregated DAE model can properly capture the average behavior of those for the original model.

Next, we show the behavior of (52a)–(52b) when we construct the cluster set as in (51b) following the network structure shown in Fig. 11(b). The initial value response is plotted in Fig. 13(a). Only the generator state trajectories are plotted because a similar trend can be observed for the generator bus voltage variables. From this figure, we see that not only the generator state trajectories of area 2, but also those of area 1 are not properly captured by their aggregated state trajectories. This is because, even though the generator states of area 1 can be aggregated by virtue of their symmetry, they are dynamically affected by the feedback effect of aggregation error from area 2. It can also be seen that a steady-state error is caused for the generator states in both areas. The reason of this steady-state error can be seen as

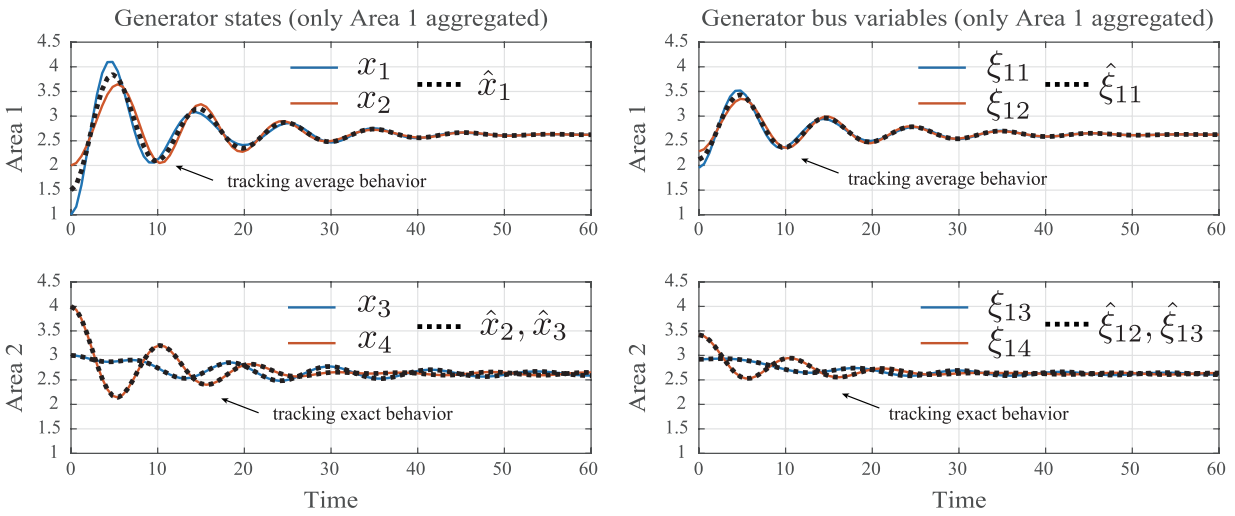

Fig. 12. ***Initial value responses of the simplified linear model (42a)–(42b) and its aggregated model (52a)–(52b) compatible with the cluster set in (51a). The system parameters and initial condition are the same as those in Fig. 10.***

follows. The steady-state (consensus) value of the aggregated DAE model, denoted by $\hat{x}_0$, can be calculated similar to (33). Therefore, $x_0 = \hat{x}_0$ holds for any $x(0)$ and $\dot{x}(0)$ if and only if (56) holds. In this case, however, the system parameters listed in the caption of Fig. 10 do not satisfy (56) for the cluster set in (51b) because $M_3 \neq M_4$ and $d_3 \neq d_4$. As shown in Fig. 13(b), the steady-state error vanishes if $M_3 = M_4$ and $d_3 = d_4$. However, the transient-state error still remains due to the asymmetry of the bus network of area 2.

As observed from this example, it is crucial to carefully select a cluster set to reduce transient error between the states of the original and aggregated DAE models. Furthermore, it is worthwhile to investigate a quantitative relation between the degree of asymmetry in the network graph and the amount of resultant transient-state error. A possible approach to such quantitative error analysis is provided in [45] and [46] from the perspective of control theory.

D. Section Summary

In Section V-A, we verified via simulations that the linearized swing model shows dynamically cohesive and synchronized behavior in both generator states and generator bus voltage variables if a certain symmetry is inherent in the network structure and physical parameters of the original DAE model. This can be seen as generalization of results in [50] for ordinary differential equations to those for DAEs describing a linearized power system model, which has not been reported in the literature. In Section V-B, we characterized this dynamic synchronism using the notion of graph symmetry defined as graph automorphism. In Section V-C, we applied this characterization to the aggregation of generator states as well as the bus voltage variables based on network clustering. It is seen that the resultant aggregated DAE model is also characterized by a weighted graph Laplacian structure associated with an aggregated bus network. The preservation of this structure enables us to interpret the aggregated DAE model as an equivalent power system where the network variables obey Kirchhoff's laws. This aggregation method with preservation of a bus network structure is a novel contribution, though several model reduction methods based on network clustering have been developed [42]–[48].

VI. STRUCTURE-BASED POWER SYSTEM CONTROL

Not only for modeling and stability analysis, graph theory has also recently emerged as an enabling tool for designing closed-loop controllers for power systems. While simple second-order models such as (7) suffice for analysis, more detailed models of generators must be considered for control design. A commonly used model for this purpose is the flux-decay model whose dynamics can be written as [23]

$$\dot{\delta} = \omega \tag{59}$$

$$M\dot{\omega} = P_m - d\omega - \frac{|V|E}{x'_{\mathrm{d}}}\sin(\delta - \angle V) + \frac{|V|^2}{2}\left(\frac{1}{x'_{\mathrm{d}}} - \frac{1}{x_{\mathrm{q}}}\right)\sin(2\delta - 2\angle V) \tag{60}$$

$$\tau_{\mathrm{do}}\dot{E} = -\frac{x_{\mathrm{d}}}{x'_{\mathrm{d}}}E + \left(\frac{x_{\mathrm{d}}}{x'_{\mathrm{d}}} - 1\right)|V|\cos(\delta - \angle V) + V_{\mathrm{fd}} \tag{61}$$

$$P + \mathrm{i}Q = \frac{E|V|}{x'_{\mathrm{d}}}\sin(\delta - \angle V) - \frac{|V|^2}{2}\left(\frac{1}{x'_{\mathrm{d}}} - \frac{1}{x_{\mathrm{q}}}\right)\sin(2\delta - 2\angle V)$$

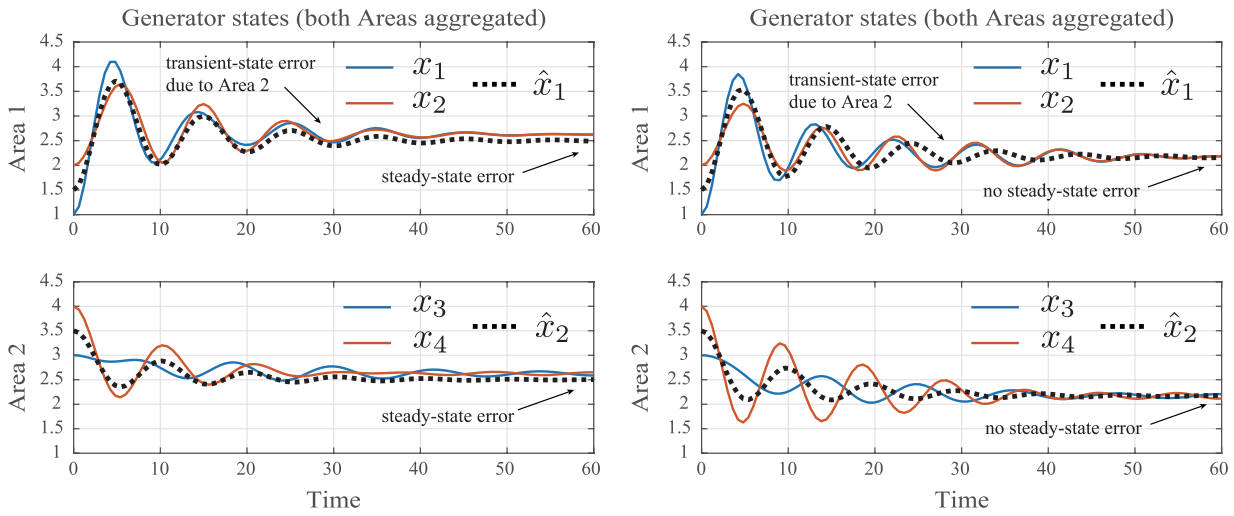

Fig. 13. *(a) Generator and aggregated generator states in the case of the same parameters as those in Figs. 10 and 12, i.e., $M_3 \neq M_4$ and $d_3 \neq d_4$. (b) Generator and aggregated generator states in the case of $M_3 = M_4 = 2$ and $d_3 = d_4 = 0.1$.*

$$+\mathbf{i}\left(\frac{E|\boldsymbol{V}|}{x'_{\mathrm{d}}}\cos(\delta - \angle \boldsymbol{V}) - |\boldsymbol{V}|^2\left(\frac{\sin^2(\delta-\angle\boldsymbol{V})}{x_{\mathrm{q}}} + \frac{\cos^2(\delta-\angle\boldsymbol{V})}{x'_{\mathrm{d}}}\right)\right)$$

where the first two state equations represent the swing dynamics, the third state equation represents electromagnetic dynamics of the generator voltage, P and Q are the active and reactive power outputs, $\boldsymbol{V}$ is the voltage phasor at the generator bus, V_{fd} is the excitor voltage, and the remaining constants denote various model parameters whose definitions can be found in any standard textbook such as [23]. The generator model is coupled with the model of an exciter consisting of an automatic voltage regulator (AVR) and a power system stabilizer (PSS) whose combined dynamics can be written as

$$\tau_{\mathrm{e}}\dot{V}_{\mathrm{fd}} = -V_{\mathrm{fd}} + V^{\star}_{\mathrm{fd}} + K_{\mathrm{a}}(|\boldsymbol{V}| - |\boldsymbol{V}|^{\star} - v + u)$$
$$\dot{\zeta} = A_{\mathrm{pss}}\zeta + B_{\mathrm{pss}}\omega, \quad v = C_{\mathrm{pss}}\zeta + D_{\mathrm{pss}}\omega$$

where the superscript * means setpoint. Again, the interested reader is referred to [23] for definitions of the state variables and model parameters. The variable u in the combined AVR/PSS model serves as a control input. Typically this input is designed using local feedback from the generator speed ω, and passing it through a lead-lag controller for enhancing damping of the oscillations in δ and ω. Traditional PSSs, however, are most effective in adding damping to the fast oscillation modes in the system, and perform poorly in adding damping to the slow or interarea oscillation modes [51]. If left undamped, interarea modes can result in transient instability, as was the case for the 1996 blackout in the U.S. west coast grid [52]. Therefore, power engineers currently are very interested in designing supplementary controllers on top of a nominal u by using state feedback from either all or selected sets of other generators spread across the grid. These types of controller are referred to as wide-area controllers [53], [54]. The use of structure for designing these controllers is explained as follows.

Let $\mathrm{Y} \in \mathbb{C}^{N\times N}$ denote the admittance matrix of the network, where N is the total number of generator and load buses. The power balance across the transmission lines follows from Kirchoff's laws as

$$0 = (\boldsymbol{Y}\boldsymbol{V})^{*} \circ \boldsymbol{V} - (P + \mathbf{i}Q) \tag{62}$$

where V, P, and Q are the stacked representations of V_k, P_k and Q_k for $k \in \{1,\ldots,N\}$. From (62), V is determined for a given P and Q. The overall dynamics of the power system can be described by the combination of every generator model (with AVR and PSS) as described above, load model, and power balance (62). Let the linearized model be denoted as

$$\dot{x} = Ax + Bu \tag{63}$$

where x is the vector of all small-signal generator states, u is the control input vector whose kth element u_k represents the kth AVR input whose output then excites the corresponding PSS. For simplicity, x is assumed to be measurable (although several wide-area control designs can also be extended to output feedback). For the linearized model (63), several papers such as [55] and [56] have posed the wide-area control problem as a sparse optimal control problem of the form: design

$$u = Kx, \qquad K \in \mathcal{S} \tag{64}$$

where $\mathcal{S}$ is a set of admissible controllers encapsulating the structured distributed nature of the controller, to minimize

$$J := \int_0^{\infty} (x^{\mathsf{T}}(t)Qx(t) + u^{\mathsf{T}}(t)Ru(t))\,dt \tag{65}$$

for a given positive–semidefinite martix Q and positive–definite matrix R, subject to (63).[1]

The goal of (64)– (65) is to promote sparsity in K for minimizing the density of the underlying communication network without sacrificing closed-loop performance much. The design in [55] and [59], for example, has sparsified K by penalizing its l_1-norm. Papers such as [60] and [61] have proposed various projection and decomposition-based control designs by which a significant portion of the communication network admits a broadcast-type architecture instead of peer-to-peer connectivity, thereby saving on the number of links. The design in [56], on the other hand, has proposed structured sparsity in light of the following general rule. Let $\mathbb{N}_G$ be the set of generator indices. For a natural number $L \leq |\mathbb{N}_G|$, consider a set of groups $\{\mathcal{G}_l\}_{l\in\{1,\ldots,L\}}$ such that $\mathcal{G}_l$ is a subset of $\mathbb{N}_G$ and $\cup_{l\in\{1,\ldots,L\}}\mathcal{G}_l = \{1,\ldots,|\mathbb{N}_G|\}$. Note that the groups are not necessarily disjoint, namely, there may exist a pair (l,l') such that $\mathcal{G}_l \cap \mathcal{G}_{l'} \neq \emptyset$. Let K_{ij} denote the (i,j)-block matrix of K, and let $\mathcal{S}$ be the set of all K such that $K_{ij} = 0$ if $(i,j) \notin \mathcal{G}_l \times \mathcal{G}_l$ for all $l \in \{1,\ldots,L\}$. The problem then is to find a wide-area controller described as (64) with this $\mathcal{S}$. The (sub)optimal set of groups $\{\mathcal{G}_l\}_{l\in\{1,\ldots,L\}}$ and the structured feedback gain K can be constructed in different ways depending on the exact objective of the controller. For the purpose of interarea oscillation damping, Jain *et al.* [56] have proposed the following construction. Modeling the fault as an impulse input, let the impulse response of the small-signal frequency of the kth generator be written as

$$\omega_k(t) = \underbrace{\sum_{i=1}^{\kappa}\left(\alpha_{ki}\exp(\lambda_i t) + \alpha_{ki}^*\exp\left(\lambda_i^* t\right)\right)}_{\text{interarea modes}} + \underbrace{\sum_{i=\kappa+1}^{|\mathbb{N}_G|}\left(\beta_{ki}\exp(\rho_i t) + \beta_{ki}^*\exp\left(\rho_i^* t\right)\right)}_{\text{local modes}}. \quad (66)$$

Assuming that the local modes are sufficiently damped by PSSs as a result of which their effect dies down quickly, the goal is to add damping to only the interarea oscillation modes. The dominance of the interarea modes is defined based on the magnitude of the modal coefficients α_{ki}. For example, consider a power system with four generators (namely $|\mathrm{N_G}| = 4$), with three interarea modes (namely $\kappa = 3$). Let the residues α_{11}, α_{21}, α_{31}, α_{32}, and α_{42} be classified as dominant residues because they satisfy $|\alpha_{ki}| \geq \mu$, where μ is a prespecified threshold. In other words, it is assumed that the interarea modes $\lambda_1$and λ_2 are substantially excited by the incoming disturbance while the third interarea mode has much poorer participation in the states. From the indices of the dominant modes, one can construct the two sets

$$\mathcal{G}_1 = \{1,2,3\}, \quad \mathcal{G}_2 = \{3,4\} \quad (67)$$

[1] The choice of the objective function J depends on the goal for wide-area control. For power oscillation damping, this function is often simply just chosen as (65); for wide-area voltage control, it can be chosen as the setpoint regulation error for the voltages at desired buses [57]; while for wide-area protection, it can be chosen as the total amount of time taken to trigger relays [58].

Table 1 Sparsity of Wide-Area Control Versus Performance Tradeoff

	Block sparsity	T	ξ
K_1	32.7%	0.42	1.05%
K_2	72.7%	1.33	7.37%
K_3	92.7%	2.68	9.74%

indicating that the generators in the first group participate dominantly in λ_1, and those in the second group participate dominantly in λ_2. This grouping information is then used to decide the topology of communication, resulting in the control input as

$$\begin{bmatrix} u_1 \\ u_2 \\ u_3 \\ u_4 \end{bmatrix} = \begin{bmatrix} K_{11} & K_{12} & K_{13} & 0 \\ K_{21} & K_{22} & K_{23} & 0 \\ K_{31} & K_{32} & K_{33} & K_{34} \\ 0 & 0 & K_{43} & K_{44} \end{bmatrix} \begin{bmatrix} x_1 \\ x_2 \\ x_3 \\ x_4 \end{bmatrix} \quad (68)$$

where the nonzero gain matrices K_{ij} are chosen to guarantee closed-loop stability, and a desired suboptimal performance. In general, the rule is that the generators inside the lth group should communicate with each other for suppressing the amplitude of oscillations excited by the lth mode λ_l. The third mode λ_3 for the above example is poorly excited, and therefore, is ignored in the control design. Following this procedure, the construction of $\mathcal{S}$ can be easily generalized to any n-generator system.

This design method was verified in [56] using the New England 39-bus, 10-generator power system model with a total of 130 states. The nonlinear power system model was excited by a three-phase fault on the line connecting buses 3 and 4, cleared after 0.1 seconds at bus 3, and after 0.15 seconds at bus 4. Based on the modal residues, the sparse structure of the controller was decided. Three different values of μ were chosen to design three controllers K_1, K_2, and K_3 with different levels of sparsity. Table 1 summarizes the results of the design, where T refers to the computation time required to solve for K, and ξ refers to the ratio of the closed-loop cost J in (65) with the sparse controller to that with the ideal LQR controller. The results show that as high as 93% sparsity can be achieved if one is willing to sacrifice 10% of the closed-loop performance. Note that since the initial condition $x(0)$ will change from one disturbance event to another, so will the group set $\{\mathcal{G}_l\}_{l\in\{1,\ldots,L\}}$. Detailed instructions on how this change can be executed in real time following a fault, and how the sets $\{\mathcal{G}_l\}_{l\in\{1,\ldots,L\}}$ (and, therefore, the wide-area controller) can vary drastically depending on the type and location of faults, are described in [56].

VII. CONCLUDING REMARKS

This tutorial overviewed a list of graph-theoretic results for modeling, stability analysis, and control of power systems. Although our discussion in this paper is mostly focused on transmission-level models, similar concepts can also be applied for analyzing dynamic and algebraic models of distribution-level power grids. Recent results

in [62], for example, have shown that Kuramoto oscillator theory can also be applied for modeling of power electronic converters that are found in abundance in distribution grids. Therefore, a relevant future work will be to extend the synchronization results and their graph-theoretic implications overviewed in Sections III and IV to such converter-interfaced power system models. Studying the impact of renewable penetration on the spectral properties of the graphs underlying the Kron-reduced model for both linear and nonlinear dynamics, and on coherency and aggregation properties of the network also constitute many open directions for future research. ■

Acknowledgements

A. Chakrabortty would like to thank A. Jain (Corning Inc.) and N. Xue (North Carolina State University) for help and insightful discussions regarding different parts of this paper.

REFERENCES

[1] A. Bose, "Smart transmission grid applications and their supporting infrastructure," *IEEE Trans. Smart Grid*, vol. 1, no. 1, pp. 11–19, Jun. 2010.

[2] *IEEE Vision for Smart Grid Controls: 2030 and Beyond*. [Online]. Available: http://ieeexplore.ieee.org/document/6577608/

[3] A. R. Bergen and D. J. Hill, "A structure preserving model for power system stability analysis," *IEEE Trans. Power Appl. Syst.*, vol. PAS-100, no. 1, pp. 25–35, Jan. 1981.

[4] D. J. Hill and G. Chen, "Power systems as dynamic networks," in *Proc. IEEE Int. Symp. Circuits Syst.*, Island of Kos, Greece, May 2006, pp. 722–725.

[5] N. Tsolas, A. Arapostathis, and P. Varaiya, "A structure preserving energy function for power system transient stability analysis," *IEEE Trans. Circuits Syst.*, vol. 32, no. 10, pp. 1041–1049, Oct. 1985.

[6] J. Jorgenson, T. Mai, and G. Brinkman, "Reducing wind curtailment through transmission expansion in a wind vision future," Nat. Renew. Energy Lab., Lakewood, CO, USA, Tech. Rep. NREL/TP-6A20-67240, Jan. 2017.

[7] S.-S. Lee, M.-U. Yang, K.-J. Kim, Y. T. Yoon, S.-I. Moon, and J.-K. Park, "Northeast Asia power system interconnection and smart grid operation strategies in South Korea," in *Proc. IEEE PES General Meeting*, Jul. 2013, pp. 1–5.

[8] W. Winter, K. Elkington, G. Bareux, and J. Kostevc, "Pushing the limits: Europe's new grid: Innovative tools to combat transmission bottlenecks and reduced inertia," *IEEE Power Energy Mag.*, vol. 13, no. 1, pp. 60–74, Jan. 2015.

[9] T. Aigner, S. Jaehnert, G. L. Doorman, and T. Gjengedal, "The effect of large-scale wind power on system balancing in Northern Europe," *IEEE Trans. Sustain. Energy*, vol. 3, no. 4, pp. 751–759, Oct. 2012.

[10] T. Sadamoto, A. Chakrabortty, T. Ishizaki, and J.-I. Imura, "Retrofit control of wind-integrated power systems," *IEEE Trans. Power Syst.*, to be published.

[11] S. Nabavi and A. Chakrabortty, "Topology identification for dynamic equivalent models of large power system networks," in *Proc. Amer. Control Conf.*, Washington, DC, USA, 2013, pp. 1138–1143.

[12] R. Madani, S. Sojoudi, and J. Lavaei, "Convex relaxation for optimal power flow problem: Mesh networks," *IEEE Trans. Power Syst.*, vol. 30, no. 1, pp. 199–211, 2015.

[13] D. Mehta, A. Ravindran, B. Joshi, and S. Kamalasadan, "Graph theory based online optimal power flow control of power grid with distributed flexible AC transmission systems (D-FACTS) devices," in *Proc. North Amer. Power Symp.*, 2014, pp. 1–6.

[14] C. Caro-Ruiz and E. Mojica-Nava, "Voltage collapse analysis in a graph theoretical framework," in *Proc. IEEE PES Innov. Smart Grid Technol. Latin America (ISGT LATAM)*, Oct. 2015, pp. 667–672.

[15] I. Dobson, "Observations on the geometry of saddle node bifurcation and voltage collapse in electrical power systems," *IEEE Trans. Circuits Syst. I, Fundam. Theory Appl.*, vol. 39, no. 3, pp. 240–243, Mar. 1992.

[16] F. Dörfler and F. Bullo, "Synchronization in complex networks of phase oscillators: A survey," *Automatica*, vol. 50, no. 6, pp. 1539–1564, 2014.

[17] S. Sundaram and C. N. Hadjicostis, "Structural controllability and observability of linear systems over finite fields with applications to multi-agent systems," *IEEE Trans. Autom. Control*, vol. 58, no. 1, pp. 60–73, Jan. 2013.

[18] B. Xu and A. Abur, "Observability analysis and measurement placement for systems with PMUs," in *Proc. IEEE Power Syst. Conf. Expo.*, Oct. 2004, pp. 943–946.

[19] A. Rahmani, M. Ji, M. Mesbahi, and M. Egerstedt, "Controllability of multi-agent systems from a graph-theoretic perspective," *SIAM J. Control Optim.*, vol. 48, no. 1, pp. 162–186, 2009.

[20] S. T. Cady, A. D. Domínguez-García, and C. N. Hadjicostis, "A distributed generation control architecture for islanded AC microgrids," *IEEE Trans. Control Syst. Technol.*, vol. 23, no. 5, pp. 1717–1735, Sep. 2015.

[21] K. R. Padiyar and S. S. Rao, "Dynamic analysis of voltage instability in AC-DC systems," *Int. J. Electr. Power Energy Syst.*, vol. 18, no. 1, pp. 11–18, Jan. 1996.

[22] J. W. Simpson-Porco and N. Monshizadeh, "Model-free wide-area monitoring of power grids via cutset voltages," in *Proc. IEEE Conf. Decision Control*, Dec. 2016, pp. 7508–7513.

[23] P. Kundur, *Power System Stability and Control*. New York, NY, USA: McGraw-Hill, 1994.

[24] J. H. Chow, Ed., *Power System Coherency and Model Reduction*. New York, NY, USA: Springer-Verlag, 2013.

[25] G. Kron, *Tensor Analysis of Networks*. New York, NY, USA: Wiley, 1939.

[26] D. S. Bernstein, *Matrix Mathematics: Theory, Facts, and Formulas*. Princeton, NJ, USA: Princeton Univ. Press, 2009.

[27] M. Fiedler, *Special Matrices and Their Applications in Numerical Mathematics*. Leiden, The Netherlands: Martinus Nijhoff, 1986.

[28] F. Dörfler, and F. Bullo, "On the critical coupling for Kuramoto oscillators," *SIAM Appl. Dyn. Syst.*, vol. 10, no. 3, pp. 1070–1099 2011.

[29] F. Dörfler, M. Chertkov, and F. Bullo, "Synchronization in complex oscillator networks and smart grids," *Proc. Nat. Acad. Sci. USA*, vol. 110, no. 6, pp. 2005–2010, 2013.

[30] Y. Kuramoto, "Self-entrainment of a population of coupled non-linear oscillators," in *Proc. Int. Symp. Math. Problems Theor. Phys.*, 1975, pp. 420–422.

[31] R. Merris, "Laplacian matrices of graphs: A survey," *Linear Algebra Appl.*, vols. 197–198, pp. 143–176, Jan./Feb. 1994.

[32] R. Olfati-Saber, J. A. Fax, and R. M. Murray, "Consensus and cooperation in networked multi-agent systems," *Proc. IEEE*, vol. 95, no. 1, pp. 215–233, Jan. 2007.

[33] W. Ren, R. W. Beard, and E. M. Atkins, "Information consensus in multivehicle cooperative control," *IEEE Control Syst. Mag.*, vol. 27, no. 2, pp. 71–82, Apr. 2007.

[34] W. Yu, G. Chen, M. Cao, and J. Kurths, "Second-order consensus for multiagent systems with directed topologies and nonlinear dynamics," *IEEE Trans. Syst. Man Cybern. B, Cybern.*, vol. 40, no. 3, pp. 881–891, Jun. 2010.

[35] B. D. MacArthur, R. J. Sánchez-García, and J. W. Anderson, "Symmetry in complex networks," *Discrete Appl. Math.*, vol. 156, no. 18, pp. 3525–3531, 2008.

[36] M. Mesbahi and M. Egerstedt, *Graph Theoretic Methods in Multiagent Networks*, Princeton, NJ, USA: Princeton Univ. Press, 2010.

[37] J. Chow and P. Kokotovic, "Time scale modeling of sparse dynamic networks," *IEEE Trans. Autom. Control*, vol. 30, no. 8, pp. 714–722, Aug. 1985.

[38] R. W. de Mello, R. Podmore, and K. N. Stanton, "Coherency-based dynamic equivalents: Applications in transient stability studies," in *Proc. Power Ind. Comput. Appl. Conf.*, New Orleans, LA, USA, Jun. 1975, pp. 23–31.

[39] J. Zaborszky, K. W. Whang, G. Huang, L. J. Chiang, and S. Y. Lin, "A clustered dynamic model for a class of linear autonomous systems using simple enumerative sorting," *IEEE Trans. Circuits Syst.*, vol. CAS-29, no. 11, pp. 747–758, Nov. 1982.

[40] L. Wang, M. Klein, S. Yirga, and P. Kundur, "Dynamic reduction of large power systems for stability studies," *IEEE Trans. Power Syst.*, vol. 12, no. 2, pp. 889–895, May 1997.

[41] N. G. Hingorani and L. Gyugyi, *Understanding FACTS: Concepts and Technology of Flexible AC Transmission Systems*. Hoboken, NJ, USA: Wiley, 1999.

[42] N. Monshizadeh and A. J. van der Schaft, "Structure-preserving model reduction of physical network systems by clustering," in *Proc. IEEE Conf. Decision Control*, Los Angeles, CA, USA, Dec. 2014, pp. 4434–4440.

[43] N. Monshizadeh, C. De Persis, A. J. van der Schaft, and J. M. A. Scherpen, "A networked reduced model for electrical networks with constant power loads," in *Proc. Amer. Control Conf.*, Boston, MA, USA, 2016, pp. 3644–3649.

[44] D. Romeres, F. Dorfler, and F. Bullo, "Novel results on slow coherency in consensus and power networks," in *Proc. Eur. Control Conf.*, 2012, pp. 742–747.

[45] T. Ishizaki, K. Kashima, J.-I. Imura, and K. Aihara, "Model reduction and clusterization of large-scale bidirectional networks," *IEEE Trans. Autom. Control*, vol. 59, no. 1, pp. 48–63, Jan. 2014.

[46] T. Ishizaki, K. Kashima, A. Girard, J.-I. Imura, L. Chen, and K. Aihara, "Clustered model reduction of positive directed networks," *Automatica*, vol. 59, pp. 238–247, Sep. 2015.

[47] N. Monshizadeh, H. L. Trentelman, and M. K. Camlibel, "Projection-based model reduction of multi-agent systems using graph partitions," *IEEE Trans. Control Netw. Syst.*, vol. 1, no. 2, pp. 145–154, Jun. 2014.

[48] B. Besselink, H. Sandberg, and K. H. Johansson, "Clustering-based model reduction of networked passive systems," *IEEE Trans. Autom. Control*, vol. 61, no. 10, pp. 2958–2973, Oct. 2016.

[49] X. Cheng, Y. Kawano, and J. M. A. Scherpen, "Reduction of second-order network systems with structure preservation," *IEEE Trans. Autom. Control*, vol. 62, no. 10, pp. 5026–5038, Oct. 2017.

[50] T. Ishizaki, R. Ku, and J.-I. Imura, "Eigenstructure analysis from symmetrical graph motives with application to aggregated controller design," in *Proc. IEEE 55th Conf. Decision Control (CDC)*, Dec. 2016, pp. 5744–5749.

[51] A. Chakrabortty and P. P. Khargonekar, "Introduction to wide-area control of power systems," in *Proc. Amer. Control Conf.*, Washington, DC, USA, Jun. 2013, pp. 6758–6770.

[52] C. W. Taylor and D. C. Erickson, "Recording and analyzing the July 2 cascading outage [Western USA power system]," *IEEE Comput. Appl. Power*, vol. 10, no. 1, pp. 26–30, Jan. 1997.

[53] N. R. Chaudhuri, D. Chakraborty, and B. Chaudhuri, "Damping control in power systems under constrained communication bandwidth: A predictor corrector strategy," *IEEE Trans. Control Syst. Technol.*, vol. 20, no. 1, pp. 223–231, Jan. 2012.

[54] J. Giri, M. Parashar, R. Avila-Rosales, and D. Wilson, "The case for using wide-area monitoring and control to improve the resilience and capacity of the electric power grid," in *Real-Time Stability in Power Systems*. New York, NY, USA: Springer-Verlag, 2014, pp. 235–278.

[55] X. Wu, F. Dörfler, and M. R. Jovanovic, "Input-output analysis and decentralized optimal control of inter-area oscillations in power systems," *IEEE Trans. Power Syst.*, vol. 31, no. 3, pp. 2434–2444, May 2016.

[56] A. Jain, A. Chakrabortty, and E. Biyik, "An online structurally constrained LQR design for damping oscillations in power system networks," in *Proc. Amer. Control Conf.*, Seattle, WA, USA, 2017, pp. 2093–2098.

[57] A. Chakrabortty, J. H. Chow, and A. Salazar, "Interarea model estimation for radial power system transfer paths with intermediate voltage control using synchronized phasor measurements," *IEEE Trans. Power Syst.*, vol. 24, no. 3, pp. 1318–1326, Aug. 2009.

[58] M. Zima, M. Larsson, P. Korba, C. Rehtanz, and G. Andersson, "Design aspects for wide-area monitoring and control systems," *Proc. IEEE*, vol. 93, no. 5, pp. 980–996, May 2005.

[59] M. Wytock, S. Sra, and J. Z. Kolter, "Fast Newton methods for the group fused lasso," in *Proc. Int. Conf. Uncertainty Artif. Intell.*, 2014, pp. 888–897.

[60] A. M. Boker, T. R. Nudell, and A. Chakrabortty, "On aggregate control of clustered consensus networks," in *Proc. Amer. Control Conf.*, Chicago, IL, USA, 2015, pp. 5527–5532.

[61] T. Sadamoto, T. Ishizaki, and J.-I. Imura, "Hierarchical distributed control for networked linear systems," in *Proc. 53rd IEEE Conf. Decision Control*, 2014, pp. 2447–2452.

[62] J. W. Simpson-Porco, F. Dörfler, and F. Bullo, "Droop-controlled inverters are Kuramoto oscillators," *IFAC Proc. Vol.*, vol. 45, no. 26, pp. 264–269, 2012.

ABOUT THE AUTHORS

Takayuki Ishizaki (Member, IEEE) was born in Aichi, Japan, in 1985. He received the B.Sc., M.Sc., and Ph.D. degrees in engineering from Tokyo Institute of Technology, Tokyo, Japan, in 2008, 2009, and 2012, respectively.

He served as a Research Fellow of the Japan Society for the Promotion of Science from April 2011 to October 2012. From October to November 2011, he was a Visiting Student at Laboratoire Jean Kuntzmann, Universite Joseph Fourier, Grenoble, France. From June to October 2012, he was a Visiting Researcher at the School of Electrical Engineering, Royal Institute of Technology, Stockholm, Sweden. Since November 2012, he has been with Tokyo Institute of Technology, where he is currently an Assistant Professor at the Department of Systems and Control Engineering. His research interests include the development of network model reduction and its applications, retrofit control and its applications, and electricity market design with distributed energy resources.

Dr. Ishizaki is a member of the Society of Instrument and Control Engineers (SICE) and The Institute of Systems, Control and Information Engineers (ISCIE). He was a finalist of the 51st IEEE CDC Best Student-Paper Award.

Aranya Chakrabortty (Senior Member, IEEE) received the Ph.D. degree in electrical engineering from Rensselaer Polytechnic Institute (RPI), Troy, NY, USA, in 2008.

From 2008 to 2009, he was a Postdoctoral Research Associate at the University of Washington, Seattle, WA, USA. He is currently an Associate Professor at the Electrical and Computer Engineering Department, North Carolina State University, Raleigh, NC, USA. His research interests are in all branches of control theory with applications to electric power systems.

Prof. Chakrabortty serves as an Associate Editor for the IEEE Control Systems Society (CSS) Conference Editorial Board (since 2012), as an Associate Editor for the IEEE Transactions on Control Systems Technology (since 2015), and as an Editor for the IEEE Transactions on Power Systems (since 2018). He received the Allen B. Dumont Prize for the best doctoral thesis in Electrical Engineering at RPI in 2008, and the NSF CAREER award in 2011.

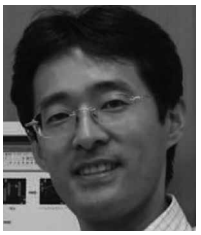

Jun-Ichi Imura (Senior Member, IEEE) received the M.E. degree in applied systems science and the Ph.D. degree in mechanical engineering from Kyoto University, Kyoto, Japan, in 1990 and 1995, respectively.

He served as a Research Associate at the Department of Mechanical Engineering, Kyoto University, from 1992 to 1996, and as an Associate Professor in the Division of Machine Design Engineering, Faculty of Engineering, Hiroshima University, Hiroshima, Japan, from 1996 to 2001. From May 1998 to April 1999, he was a Visiting Researcher at the Faculty of Mathematical Sciences, University of Twente, Enschede, The Netherlands. Since 2001, he has been with Tokyo Institute of Technology, Tokyo, Japan, where he is currently a Professor at the Department of Systems and Control Engineering. His research interests include modeling, analysis, and synthesis of nonlinear systems, hybrid systems, and large-scale network systems with applications to power systems, ITS, biological systems, and industrial process systems.

Prof. Imura served as an Associate Editor of *Automatica* (2009–2017), *Nonlinear Analysis: Hybrid Systems* (2011–2016), and the IEEE Transactions on Automatic Control (2014–2016). He is a member of the Society of Instrument and Control Engineers (SICE), The Institute of Systems, Control and Information Engineers (ISCIE), and The Robotics Society of Japan.